Atmos. Chem. Phys., 8, 4027–4048, 2008
www.atmos-chem-phys.net/8/4027/2008/

Atmospheric Chemistry and Physics

Fast airborne aerosol size and chemistry measurements above Mexico City and Central Mexico during the MILAGRO campaign

P. F. DeCarlo[1,2,*], E. J. Dunlea[1], J. R. Kimmel[1], A. C. Aiken[1,3], D. Sueper[1], J. Crounse[4], P. O. Wennberg[4], L. Emmons[5], Y. Shinozuka[6], A. Clarke[6], J. Zhou[6], J. Tomlinson[7], D. R. Collins[7], D. Knapp[5], A. J. Weinheimer[5], D. D. Montzka[2], T. Campos[5], and J. L. Jimenez[1,3]

[1]Cooperative Institute for Research in Environmental Science (CIRES) University of Colorado, Boulder, CO, USA
[2]Department of Atmospheric and Oceanic Science, University of Colorado at Boulder, Boulder, CO, USA
[3]Department of Chemistry and Biochemistry, University of Colorado at Boulder, Boulder, CO, USA
[4]California Institute of Technology, Pasadena, CA, USA
[5]National Center for Atmospheric Research, Boulder, CO, USA
[6]Department of Oceanography, University of Hawaii, USA
[7]Department of Meteorology, Texas A&M University, College Station, TX, USA
[*]now at: Laboratory of Atmospheric Chemistry, Paul Scherrer Institute, Switzerland

Received: 22 November 2007 – Published in Atmos. Chem. Phys. Discuss.: 20 December 2007
Revised: 20 June 2008 – Accepted: 20 June 2008 – Published: 25 July 2008

Abstract. The concentration, size, and composition of non-refractory submicron aerosol (NR-PM_1) was measured over Mexico City and central Mexico with a High-Resolution Time-of-Flight Aerosol Mass Spectrometer (HR-ToF-AMS) onboard the NSF/NCAR C-130 aircraft as part of the MILAGRO field campaign. This was the first aircraft deployment of the HR-ToF-AMS. During the campaign the instrument performed very well, and provided 12 s data. The aerosol mass from the AMS correlates strongly with other aerosol measurements on board the aircraft. Organic aerosol (OA) species dominate the NR-PM_1 mass. OA correlates strongly with CO and HCN indicating that pollution (mostly secondary OA, SOA) and biomass burning (BB) are the main OA sources. The OA to CO ratio indicates a typical value for aged air of around 80 μg m^{-3} (STP) ppm^{-1}. This is within the range observed in outflow from the Northeastern US, which could be due to a compensating effect between higher BB but lower biogenic VOC emissions during this study. The O/C atomic ratio for OA is calculated from the HR mass spectra and shows a clear increase with photochemical age, as SOA forms rapidly and quickly overwhelms primary urban OA, consistent with Volkamer et al. (2006) and Kleinman et al. (2008). The stability of the OA/CO while O/C increases with photochemical age implies a net loss of carbon from the OA. BB OA is marked by signals at m/z 60 and 73, and also by a signal enhancement at large m/z indicative of larger molecules or more resistance to fragmentation. The main inorganic components show different spatial patterns and size distributions. Sulfate is regional in nature with clear volcanic and petrochemical/power plant sources, while the urban area is not a major regional source for this species. Nitrate is enhanced significantly in the urban area and immediate outflow, and is strongly correlated with CO indicating a strong urban source. The importance of nitrate decreases with distance from the city likely due to evaporation. BB does not appear to be a strong source of nitrate despite its high emissions of nitrogen oxides, presumably due to low ammonia emissions. NR-chloride often correlates with HCN indicating a fire source, although other sources likely contribute as well. This is the first aircraft study of the regional evolution of aerosol chemistry from a tropical megacity.

Correspondence to: J. L. Jimenez
(jose.jimenez@colorado.edu)

1 Introduction

Aerosols are important components of the earth system. Some of the effects of aerosols are reduction in visibility (Watson, 2002), deterioration of human health (Pope and Dockery, 2006), deposition of pollutants to ecosystems (Bytnerowicz and Fenn, 1996), and direct and indirect effects on the radiative balance of the climate system. Currently, aerosols and their associated direct and indirect effects contribute the largest uncertainty to the radiative forcing of the

climate system (IPCC, 2007). Organic species account for a large fraction of the submicron aerosol mass at most locations (Zhang et al., 2007a) and are especially poorly understood. Urban areas are large sources of aerosols and aerosol precursors. Pollution from megacities and large urban areas is important not only for local effects on health, visibility, and ecosystems/crops but also because of their collective influence in regional to global scale atmospheric chemistry and radiative forcing (Lawrence et al., 2007; Madronich, 2006).

The Megacity Initiative: Local and Global Research Observations (MILAGRO) took place in and around Mexico City during March of 2006. The Megacity Impacts on Regional and Global Environment (MIRAGE-Mex) was the component of the MILAGRO campaign under US NSF sponsorship, and included several aircraft platforms and ground sites. The MILAGRO campaign was designed to study the chemical characterization and transformation of pollutants from the Mexico City urban area to regional scales in a pseudo-lagrangian framework. A High-Resolution Time-of-Flight Aerosol Mass Spectrometer (HR-ToF-AMS) (DeCarlo et al., 2006) was deployed for the first time on an aircraft platform onboard the National Science Foundation / National Center for Atmospheric Research (NSF/NCAR) C-130 aircraft.

Air pollution in Mexico City has been studied for many years. An overview and detailed list of the studies in Mexico City from 1960–2000 is given by Raga et al. (2001). Important conclusions include the need for size-resolved composition measurements of $PM_{2.5}$ aerosol, as well as the need of vertical measurements of aerosol species. More recent studies in Mexico City have added to our understanding of Mexico City pollution. Salcedo et al. (2006) conclude that organics dominate $PM_{2.5}$ inside the city during the MCMA-2003 campaign, and a significant fraction of the organics are oxygenated organic aerosol (OOA). Sulfate showed a more regional behavior while nitrate was mostly produced from local photochemistry. Non-refractory (NR) chloride was present in small levels with a diurnal cycle peaking in the morning, but also showed some very large plumes that were not associated with OA. The inorganic acids were neutralized by ammonium most of the time, although some periods with ammonium deficit were also observed when sulfate was high. Volkamer et al. (2006) show that secondary organic aerosol (SOA) from urban sources is produced rapidly and about 8 times more efficiently in the city than an SOA model predicted. Although only one case study is presented, the paper states that similar conclusions were obtained for several other days simulated. This study extended previous results about SOA underprediction over regional scales (de Gouw et al., 2005; Johnson et al., 2006a; Heald et al., 2005) to shorter time scales and the urban environment. Kleinman et al. (2008) analyzed the aerosol evolution with photochemical age during MILAGRO over the urban area and near outflow and confirm the results of Volkamer et al. (2006).

Wildfires and biomass burning (BB) have also been identified as important sources of particulate matter in Mexico City. Bravo et al. (2002) found a correlation between estimated emissions from wildfires and both Total Suspended Particles (TSP) and PM_{10} for the years 1992–1999. During the Mexico City Metropolitan Area campaign in 2003 (MCMA-2003) biomass burning was identified as an important source of fine particles, and especially for OA and also mineral matter and black carbon, but with no enhancement of nitrate, sulfate, or ammonium (Johnson et al., 2006b; Molina et al., 2007; Salcedo et al., 2006). Recent results from the MILAGRO campaign also suggest that biomass burning contributed significantly to the gas and particle pollution in the city basin and outflow, although the magnitude of the impacts of fires is the subject of debate (Moffet et al., 2007; Stone et al., 2008; Querol et al., 2008; Yokelson et al., 2007). A source apportionment study using trace metals, inorganics, EC, and OC at many locations in and around Mexico City for total $PM_{2.5}$ and PM_{10} did not identify biomass burning as a source (Querol et al., 2008). However, specific tracers of this source (e.g., WSOC, water-soluble K, levoglucosan) were not included in this study, and thus biomass burning emissions were probably mixed with other emission sources in the source apportionment analysis (M. Viana, personal communication, 2007). A different source apportionment study of fine organic aerosol reports that BB made a highly variable contribution in time accounting on average for 16% and 32% of the ambient organic carbon (OC) at the urban (T0) and rural (T1) ground supersites respectively (Stone et al., 2008). ^{14}C measurements indicate a significant fraction of modern carbon in the organic aerosol measured at the T0 site, part of which likely originates from urban sources such as trash burning and cooking (Aiken et al., 2007a; Gaffney et al., 2008).

The meteorology of the Mexico City basin has been characterized in earlier field campaigns. The meteorology of the basin is very complex in response to synoptic, land/sea, and orographic forcings (de Foy et al., 2006; Fast and Zhong, 1998). These field campaigns examined venting timescales of the basin and concluded that typically the basin vents on timescales less than one day (de Foy et al., 2006; Fast and Zhong, 1998). Mixing heights during the MCMA-2003 campaign were typically around 3000 m and vigorous vertical mixing implied pollutants were well mixed in the boundary layer during the day (de Foy et al., 2006). A recently published study examines the basin scale wind transport during the MILAGRO campaign, identifying six episode types and compares the meteorological conditions in March 2006 with previous 10 years (de Foy et al., 2008). An overview of the large-scale meterology during the MILAGRO campaign is presented in Fast et al. (2007) and identifies 3 general regimes. 1–14 March is the first regime and is characterized by sunny and dry conditions. The second regime from 14–23 March saw an increase in humidity and the development of afternoon convection, which slowly diminished

as the atmosphere became drier. The third regime (24–31 March) began with a cold surge, saw increased precipitation, and a decrease in the frequency and intensity of fires.

The C-130 performed 12 research flights (RFs) during the MILAGRO campaign. Flight altitudes were typically less than 6 km above sea level (ASL) (∼96% of data), and approximately 97% of city data (defined in Sect. 3.2) were taken at less than 2 km radar altitude. Vigorous turbulent mixing in the boundary layer implies a well mixed boundary layer over Mexico City during the afternoon. The regional data average altitude is 4.0 km above sea level (a.s.l.) and 3.2 km radar altitude (above the ground). For this paper the focus will be on RFs 2, 3, and 12 (8, 10 and 29 March 2006, respectively). Data will also be presented from RFs 1, 9, 10, and 11 from the 4, 23, 26 and 28 March 2006. RFs 2, 3, and 12 all had city and regional components in their flight patterns. RF 1 had a city and regional component, but not all instruments were working on the C-130. RF 9 was a flight to the Yucatan Pennisula, and did not contain a city component. RF 10 was cut short due to mechanical problems with the aircraft, and the majority of the flight was spent at high altitude. RF 11 was a flight designed to measure the morning transition of photochemistry and did not sample in the city basin. During RFs 4-8 a leak in the shared inlet system did not allow quantitative measurements of aerosol chemistry; when possible mass fractions of the measured AMS chemical species were reported to the database, however they have not been included in this paper.

In this paper, we present, the results of the measurements of non-refractory submicron aerosol chemistry from the HR-ToF-AMS in the C-130 which indicate that organic aerosols (OA) are the largest NR chemical component, with nitrate, sulfate, ammonium, and chloride also making significant contributions. Different aerosol species have different spatial distributions and tracer correlations, indicating influences from different sources and processes. A large fraction of the organic aerosol is oxidized, with an oxygen-to-carbon atomic ratio (O/C) that increases with distance from the city approaching a ratio of 0.9 away from the basin. Organic O/C can be used as a qualitative "photochemical clock". Finally a detailed case study of RF 2 is presented to assemble all of these results into a coherent and detailed picture of submicron aerosol over and around Mexico City. Quantitative apportionment of OA sources will be addressed in a subsequent publication.

2 Methods

2.1 Instrumentation

2.1.1 HR-ToF-AMS

The HR-ToF-AMS has been described in detail previously (DeCarlo et al., 2006). It improves upon previous versions of the AMS (Drewnick et al., 2005; Jayne et al., 2000; Canagaratna et al., 2007) by the use of a high-resolution mass spectrometer that allows the determination of the elemental composition of most ions, while previous AMS versions can only determine the total signal at each integer mass. In the rest of the paper we will refer to the HR-ToF-AMS as "AMS" for brevity. The AMS sampled non-refractory submicron aerosol (NR-PM_1) during the research flights. Data were acquired in two acquisition modes (Jimenez et al., 2003): Particle Time-of-Flight mode (PToF) which allows for particle sizing, and Mass Spec (MS) mode, which produces species concentrations and a complete mass spectrum of the non-refractory submicron mass with no size information, but with higher sensitivity than the PToF mode. For most of the campaign data was averaged and saved every 12 s. Data was also saved at longer time intervals (∼30–45 s) early in the campaign, and sometimes a "plume-mode" was utilized which consisted of 3 s save intervals of MS mode only (no particle sizing). The HR-ToF-AMS was run exclusively in the V-mode of ion flight for the mass spectrometer, which is about a factor of 10 more sensitive than the alternative W-mode. V-mode operation has lower resolution than W-mode, but still maintains high enough resolution to separate most ions of the same nominal mass, and especially reduced vs. oxidized organic fragments (DeCarlo et al., 2006). This instrument was installed towards the rear of the C-130 (http://mirage-mex.acd.ucar.edu/Measurements/C130/Images/C-130_layout.png) and shared an inlet system with the Georgia Tech Particle into Liquid Sampler (PILS). The inlet is described in more detail elsewhere (Dunlea et al., 2008). Briefly, the inlet was mounted in the belly of the aircraft and consisted of a near isokinetic shallow conical diffuser into a 2.54 cm (1.0 inch) diameter stainless steel tube with a smooth 90° bend into the cabin floor. The flow was then isokinetically subsampled into the AMS line (8 l per min) and PILS (30 l per min). A pressure controlled inlet was used just before the AMS (Bahreini et al., 2008), to eliminate the fluctuations in aerosol sizing and transmission efficiency due to changing pressures in the aerodynamic lens of the instrument. The PCI used a setpoint of 350 Torr, with a 180 micron orifice upstream, and a 150 micron orifice in the lens of the AMS. This allows for sampling up to ∼6.5 km without the need for flow or sizing corrections to the raw AMS data. The transmission of particle sizes into the AMS was determined by the AMS inlet (critical orifices and aerodynamic lens) as the losses in the plane inlet and tubing were small for the AMS size range (Dunlea et al., 2008). The residence time between the inlet tip and the AMS was ∼4 s (of which 3.2 s was in the PCI), and the flow warmed up to cabin temperature due to ram heating in the inlet and heat transfer (ΔT ∼2–35°C for aircraft altitudes below 4 km). This may have led to some evaporation of aerosol components (Murphy et al., 2007), which would be more important for ammonium nitrate and chloride, less important for organics, and negligible for ammonium

sulfate (Huffman et al., 2008b). Further information on AMS data processing is given in Sect. 2.3.

2.1.2 Nephelometer

Total and submicrometer aerosol scattering coefficients were measured at 450, 550 and 700 nm using two TSI model 3563 3-wavelength integrating nephelometers (Anderson et al., 1996; Heintzenberg and Charlson, 1996; Anderson et al., 2003). The submicrometer TSI nephelometer employed a 1-μm aerodynamic impactor maintained at 30 lpm by an Alicat Scientific volumetric flow controller. While the measurements were made every second, sample air residence time inside the nephelometers was about 10 s. The noise over 10 s at 550 nm is estimated to be 0.3 Mm^{-1} (Anderson et al., 1996). The instrument relative humidity was usually lower than 30%. The scattering coefficients were detected over 7–170°, and corrected for 0–180° using the measured wavelength dependence as a surrogate for the particle size after Anderson and Ogren (1998). For the submicron (PM_1) scattering, this angular truncation correction is typically less than 10%, and contributes negligible (<3%) uncertainty. Gas calibration results in a smaller (+/−1%) systematic error (Anderson et al., 1996). The aerosol inlet for the nephelometer was a shrouded solid diffuser maintained at isokinetic flow ±5% and aspirated at about 100 lpm. The aerodynamic 50% size cut was 5 μm (McNaughton et al., 2007).

2.1.3 Optical Particle Counter (OPC)

An optical particle counter (OPC, a modified LAS-X, Particle Measurement Systems, Boulder, Colorado) measured the dry (RH<30%) aerosol size distribution between 0.1 μm and about 10 μm (Clarke, 1991). The He-Ne laser operates at 633 nm detecting light scattered by individual particles over 35–145°. The particle size up to 2 μm was calibrated with polystyrene latex spheres whose refractive index is 1.59. For calibrating the coarse mode, glass beads with a refractive index of 1.54 were also used. The data was obtained every 3 s, but averaged over 30 s to reduce error due to low counting statistics at about 1 μm or larger.

2.1.4 Scanning Mobility Particle Sizer (SMPS)

The Texas A&M SMPS (Wang and Flagan, 1990) measured the size distribution of particles between 0.012 and 0.67 μm mobility diameter once every 1.5 min. A high flow differential mobility analyzer (Stolzenburg et al., 1998) is used in the SMPS with sample and sheath flow rates of 1.5 and 15 l per min, respectively. The sampled aerosol was dried to below 10% RH prior to classification using a Nafion tube bundle. The SMPS was located adjacent to, and shared an inlet with, the nephelometer and Single particle soot photometer (SP2). The "apparent" aerosol volume (DeCarlo et al., 2004) was calculated from the SMPS size distributions with the assumption of spherical particles. This volume would be biased high if a significant fraction of the particles were non-spherical, which is however not expected due to the large fraction of secondary species.

2.1.5 HCN

The Caltech CIMS (Crounse et al., 2006) measured selected product ions on the C-130 via reaction of the reagent ion CF_3O^- with analytes directly in air. HCN is measured by monitoring the product ion at m/z 112, which is the cluster of CF_3O^- with HCN. The sensitivity to HCN is dependent on the water vapor mixing ratio. Sensitivity changes due to water vapor changes are corrected for using the dewpoint hygrometer water measurement from the C-130 aircraft, and a water calibration curve that has been generated though laboratory measurements. Non-water sensitivity changes are corrected for using in-flight standard addition calibrations of H_2O_2 and HNO_3 (other species measured by the CIMS) and proxied to laboratory calibrations of HCN. The detection limit (S/N=1) for HCN for a 0.5 s integration period is better than 15 pptv for moderate to low water vapor levels (H_2O mixing ratio $\leq$0.004).

2.1.6 CO

The NCAR/NSF C-130 CO vacuum UV resonance fluorescence instrument is similar to that of Gerbig et al. (1999). The MILAGRO data have a 3 ppbv precision, 1-s resolution, and a typical accuracy of ±10% for a 100 ppbv ambient mixing ratio.

2.1.7 NO_x, NO_y measurement

NO_x (NO and NO_2) and NO_y (total reactive nitrogen) were measured (along with O_3) using the NCAR 4-channel chemiluminescence instrument, previously flown on the NASA WB-57F (Ridley et al., 2004). NO_y was measured via Au-catalyzed conversion of reactive nitrogen species to NO, with a time response of about 1 s. NO_2 was measured as NO following photolytic conversion of NO_2, with a time response of about 3 s due to the residence time in the photolysis cell. NO was measured with an identical time response due to use of a cell with an identical residence time. NO and NO_2 are reported at 1-s. For NO, NO_2, and NO_y, the precision of a 1-s value is near 15 pptv. The overall estimated uncertainties of 1-s values are ±(15+7% of the mixing ratio) pptv for NO, ±(15+10% of the mixing ratio) pptv for NO_2, ±(15+15% of mixing ratio) pptv for NO_y.

2.1.8 MOZART model

A simulation of MOZART-4 (Model for Ozone and Related chemical Tracers, version 4) (Emmons et al., 2008[1]) was run where tracers that represented the CO emissions from Mexico City for each day were included. MOZART-4 was driven with NCEP/GFS (National Centers for Environmental Prediction Global Forecast System) meteorological fields at a horizontal resolution of T170 (0.7°). The emissions are from the Mexico National Emissions Inventory for 1999 (http://www.epa.gov/ttn/chief/net/mexico.html, as gridded by M. Mena, U. Iowa) and the tracers include the emissions between 18–20° N and 98–100° W.

2.2 Ground supersites

The ground supersites, named T0, T1, and T2 are described in Fast et al. (2007). Some additional information on the ground supersites is given in Querol et al. (2008) and Stone et al. (2008). Briefly T0 was inside the city, and T1 and T2 were outside the city to the northeast about 30 and 63 km away from T0 respectively. The names were chosen to indicate the relative ages of air for pseudo-lagrangian experiments when city air flowed to the northeast. A more detailed discussion of these sites will be given in the forthcoming MILAGRO overview paper (Molina et al., 2008[2]). Notably at the T0 supersite another HR-ToF-AMS was deployed jointly by the Jimenez group and Aerodyne (Aiken et al., 2007a, 2008).

2.3 AMS data processing

2.3.1 AMS calibrations

Procedures for AMS calibration can be found in previous publications (Allan et al., 2003, 2004; Jimenez et al., 2003; Kimmel et al., 2006). The amplification factor of the microchannel plate detector (MCP) was measured every day the instrument was in use ("single ion calibration"). Due to the stability and reproducibility of the single ion throughout the campaign a single average value was used for the entire campaign. The lack of MCP degradation is likely due to the very limited instrument use, ~120 h total, equivalent to only 5 days of operation in a ground-based field campaign. Ionization efficiency (IE) calibrations were performed 6 times during the campaign. Due to customs issues the calibration equipment was not delivered until 10 days into the campaign, thus the IE for the first 3 flights was assumed to be the same, and was determined by a calibration made on 12 March 2006. Over the course of the campaign the IE calibration values varied by 20%, but varied by smaller amounts from flight to flight. 20% is therefore an upper limit to the uncertainty introduced by not having calibration equipment for the first three flights. IE values for the rest of the flights were determined from calibrations bracketing the flights. All AMS data was converted to mass loading at standard temperature and pressure (STP, 273 K and 1013.25 hPa). Measured AMS mass was converted to volume using the assumption that species volume is additive (Eq. 4 of DeCarlo et al. (2004)). For this conversion the densities of the species were assumed to be 1.78, 1.72, and 1.52 g cm^{-3} for ammonium sulfate, ammonium nitrate, ammonium chloride respectively (Lide, 2007). A density of 1.27 g cm^{-3} was used for organics, based on the measured value from Cross et al. (2007).

2.3.2 AMS data processing

AMS Data was processed in the Igor Pro 6.0 Software (Wavemetrics Inc. Lake Oswego, Oregon) using the standard ToF-AMS Data Analysis toolkit, ("Squirrel", http://cires.colorado.edu/jimenez-group/ToFAMSResources/ToFSoftware/SquirrelInfo/). The particle collection efficiency (CE) for the AMS was assumed to be 0.5 unless there was evidence of acidic aerosol (see Fig. 2 for comparisons of AMS results with those from other instruments). In cases of acidic aerosol, the CE was increased proportional to the mass fraction of sulfuric acid (CE=1) to ammonium bisulfate (CE=0.5) (Canagaratna et al., 2007; Quinn et al., 2006; Takegawa et al., 2005). The integration of total signals for individual ions ("high-resolution sticks," e.g. $C_2H_3O^+$ and $C_3H_7^+$ at m/z 43) from raw mass spectral data was carried out using the "Pika" module of Squirrel developed by our group (http://cires.colorado.edu/jimenez-group/ToFAMSResources/ToFSoftware/PikaInfo/), which implements the procedures described in DeCarlo et al. (2006). Sticks for spectra acquired in open (particles + air + mass spectrometer background) and closed (only background) modes were calculated. Particle + air signal for each ion was determined by the difference of the open signal and the closed signal. Air contributions to individual ions (e.g. CO_2^+ at m/z 44) were subtracted from the total signal at that ion. Variations in the gas-phase CO_2 would produce only a very small effect in the aerosol CO_2^+ ion signal. The typical gas-phase CO_2 background of ~380 ppm is equivalent to ~100 ng m^{-3} of organic-equivalent (org.-eq. (Zhang et al., 2005a)) aerosol signal at m/z 44. This signal is subtracted from ~2600 ng m^{-3} of org.-eq. m/z 44 aerosol signal in the city and ~1000 ng m^{-3} in regional air. Variations on the order of 40 ppm for gas-phase CO_2 would change its contribution to total m/z 44 by +/− 10 ng m^{-3}, which is within the noise of the measurement. Note that this correction can be much more important for studies with low OA concentrations.

[1]Emmons, L. K., Hess, P. G., Lamarque, J.-F., Pfister, G. G., Fillmore, D., Granier, C., Guenther, A., Kinnison, D., Laepple, T., Orlando, J., Tie, X., Tyndall, G., Walters, S., et al.: Impact of Mexico City emissions on regional air quality from MOZART-4 simulations, Atmos. Chem. Phys., in preparation, 2008.

[2]Molina, L. T., Madronich, S., Gaffney, J. S., et al.: An Overview of the MILAGRO Campaign: Mexico City Emissions and Their Evolution, Atmos. Chem. Phys. Discuss., in preparation, 2008.

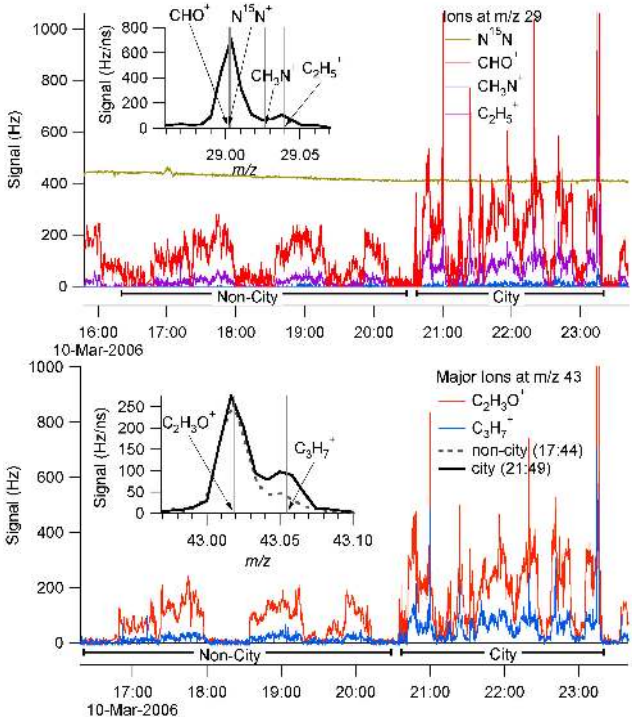

Fig. 1. High-resolution ion signals at m/z 29 and 43 for RF 3 (10 March 2006). The insets shows individual 12-s high resolution mass spectra for m/z 29 and 43. For m/z 43, the oxygen-containing fragment dominates the total signal in both the city and non-city case, however the intensity of the $C_3H_7^+$ ion increases in the city, indicating additional presence of more reduced aerosol species such as primary traffic and biomass burning emissions.

A correction at m/z 29 was also necessary, as the 2 most intense peaks CHO^+ and $^{15}NN^+$ (29.00274 and 29.00318, respectively), cannot be separated at the resolution of the instrument. $N^{15}N^+$ was calculated as a constant fraction of the N_2^+ signal at m/z 28 from calibrations with a particle filter, with the remaining signal assigned to the CHO^+ ion. Two other peaks, corresponding to $C_2H_5^+$ and CH_3N^+at m/z 29 were also resolved from the above two ions. Figure 1 shows ion signals at m/z 29 and 43 during research flight 3. Traces of the ion signals for this flight are shown and insets show the mass spectra for these m/z for one 12 s data point. The inset for m/z 43 shows 2 different mass spectra corresponding to 2 different portions of the flight; one in the city and one in the outflow. From this it is clear that the $C_2H_3O^+$ fragment is proportionately larger than the $C_3H_7^+$ fragment, indicative of the larger contribution of oxygenated species (likely SOA) in the outflow and of more reduced species (such as traffic exhaust, biomass burning, and less aged SOA) over the city.

2.3.3 Calculation of light scattering from AMS Data

AMS total size distributions from PToF mode were averaged to a 5 minute timebase for RFs 1, 2, 3, 9, 10 11, and 12. The total NR size distribution was converted to a number distribution vs. volume-equivalent diameter ($dN/d\log d_{ve}$), assuming spherical particles and using the bulk density of the aerosol calculated from the chemical composition for each 5 min average, according to the conversions detailed in DeCarlo et al. (2004). Scattering was calculated for this distribution using the routine of Bohren and Huffman (1983) translated into Igor (C. Brock, NOAA, personal communication, 2006). We used a refractive index of 1.54, which is the average of the refractive indices for Ammonium Sulfate (1.55), and organics (1.53) (Hand et al., 2002; Kleinman et al., 2007) and calculated scattering at 550 nm to compare to the Nephelometer, which measured submicron scattering at that wavelength.

2.3.4 Elemental analysis of organic aerosol from AMS data

Elemental analysis was performed on the high-resolution data following the method described in Aiken et al. (2007b, 2008). Inorganic and air ions were removed so only organic ions were included in the calculation of elemental ratios. Oxygen-to-carbon atomic ratios of the organic aerosol (O/C) and hydrogen-to-carbon (H/C) were determined, as well as the organic mass-to-organic carbon ratio (OM/OC). The nitrogen-to-carbon ratio was calculated, however the V-mode does not have enough resolution to reliably quantify some N-containing ions, so the absolute N/C ratio is not reported, although it is used in the OM/OC calculation. W-mode data from the T0 supersite in Mexico City show that organic N/C is typically more than an order of magnitude smaller than the O/C (Aiken et al., 2008), comparable to the N/C ratio found on the C-130. Thus errors in the reported OM/OC due to imprecision in the N/C ratios derived here should be small. Organonitrates and organosulfates can produce nominally "inorganic" ions in the AMS (e.g. NO^+, NO_2^+, SO^+, SO_2^+). Ignoring these ions will result in a negative bias on the O/C and OM/OC. However the analysis of the stoichiometric neutralization of ammonium vs. nitrate, sulfate, and chloride (discussed below, see also Zhang et al. (2007b)) suggests that the contribution of these types of species (and thus the associated errors in O/C and OM/OC) is small. To avoid the effect of noise at low OA concentrations, ratios are only reported when the OA mass was larger than 2 $\mu g\,m^{-3}$.

3 Results and discussion

3.1 Aerosol Measurement Intercomparisons

Data were converted to the timebase of the slower measurement when comparing with different instruments. The AMS mass and calculated volume and the Nephelometer submicron scattering were reported at approximately 12 s per data point, and for comparisons Nephelometer data was interpolated to the AMS timebase. The SMPS data was recorded on

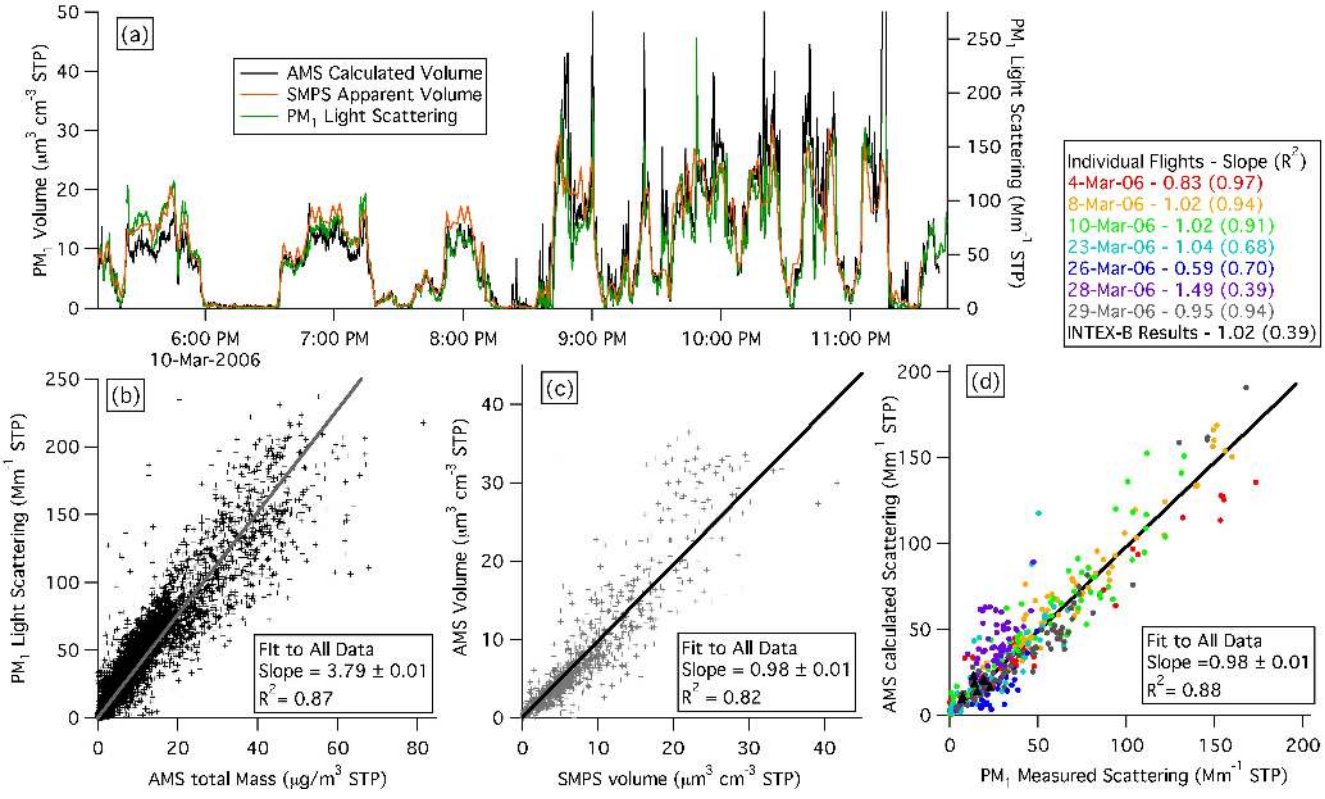

Fig. 2. **(a)** Time series from RF 3 (10 March 2006) of AMS calculated volume, SMPS apparent volume, and PM_1 light scattering, all on their native timebases. **(b)** Scatter plot of submicron light scattering as measured at 550 nm by the Nephelometer vs the AMS total mass. Data is interpolated to the AMS timebase and the majority of data points in the plot are 12 s averages. **(c)** Scatter plot of volume calculated from the AMS mass and composition-dependent density, against the apparent volume calculated from the SMPS distribution assuming particle sphericity. The AMS data in this plot has been averaged to the 96 second SMPS timebase. A slope close to 1 and an R^2 of 0.82 indicate good general agreement. **(d)** Calculated scattering from 5-min AMS size distributions and Mie theory versus average measured scattering by the Nephelometer over the same period. 27 data points out of 507 total points were eliminated due to low loading resulting in unphysical size distributions from the AMS. Reported errors in slopes in plots b-d are the 1-σ estimate for the fitted variables returned from the fitting algorithm.

a 96 s timebase, for this comparison AMS data was averaged to the SMPS timebase. The calculation of scattering from AMS size distribution data was done on a 5 min time grid as the size distributions have lower signal to noise ratios than total mass concentrations and require more time integration. Figure 2a shows a timeseries from RF 3 (10 March 2006) for calculated AMS volume, SMPS apparent volume, and measured PM_1 Light Scattering. All data are shown in Fig. 2a at their native sampling resolution, and high correlation among the measurements is seen. Although only one flight is shown, other flights show similar agreement. Correlations between the different measurements for the whole campaign are discussed in the following sections. Note that data from takeoff and landing were excluded from these comparisons since the inlet for the AMS was in a different location on the aircraft than the Nephelometer and SMPS, and particles generated by the landing gear and exhaust are sampled differently for these portions of the flights.

3.1.1 AMS vs. Nephelometer comparison

A direct comparison of Nephelometer Scattering to NR-submicron aerosol mass for the entire MILAGRO campaign shows high correlation (see Fig. 2b). The slope of the linear regression (3.79 m^2/g) is equivalent to the Mass Scattering Efficiency (MSE), and is in good agreement with the range of dry MSE values of 3.6 ± 1.3 m^2/g reported by Shinozuka et al. (2007). Based on preliminary data, black carbon makes up 1–3% of the submicron mass during MIRAGE (R. Subramanian, DMT, personal communication), and would make up slightly less of the submicron volume due to the higher density values for black carbon (Park et al., 2004) in relation to the dominant organic constituents; consequently the AMS mass or calculated volume is not expected to be significantly impacted by the exclusion of black carbon. Some of the scatter can be explained by differences in the exact size cuts of both instruments, and of sampling timebase,

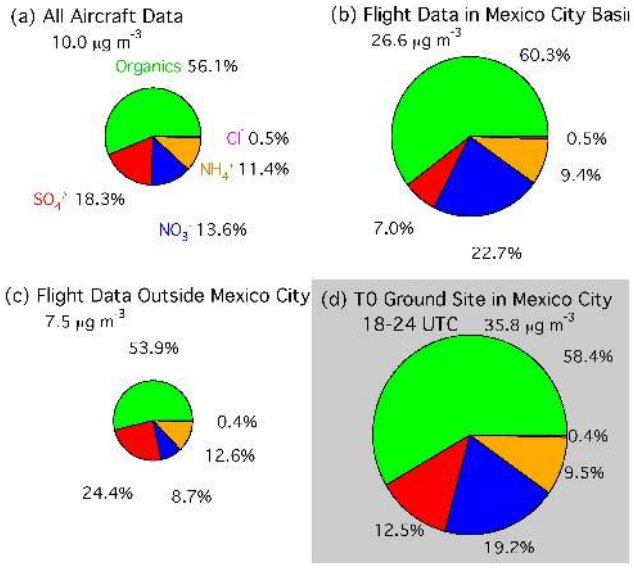

Fig. 3. Average chemical composition of NR-PM_1 in different regions. Mass concentrations are given in $\mu g\,m^{-3}$ STP (273 K, 1 atm). Panel **(d)** has a gray background to differentiate the ground data from the aircraft data **(a)** Average of whole MIRAGE aircraft campaign. **(b)** Average of MIRAGE data when flying directly over Mexico City. **(c)** Average of MIRAGE excluding all points over Mexico City. (d) Average measured at the ground at the T0 Supersite, between the hours of 18:00–24:00 UTC (12:00–18:00 local time). The time period was chosen for comparison purposes, as this is when the C-130 typically flew over the city (see text). The area of each pie is proportional to average mass concentration.

frequency, and different inlet locations on the aircraft. The AMS sampled in MS mode approximately half of the time, while the Nephelometer was sampling continuously. Short plumes (∼6 s or less equivalent to approximately 600 m at 100 m/s) could be missed by the AMS or be sampled and be non-representative of the average mass loading for the period in question. The regression of submicron Nephelometer scattering to AMS calculated volume gave a slope (Volume Scattering Effciency) of 5.50 $m^2\,cm^{-3}$ (R^2=0.86).

3.1.2 AMS and SMPS volume comparison

Figure 2c shows a scatter plot of AMS calculated volume vs. SMPS apparent volume for all overlapping data during MIRAGE. Again, good agreement is found with a slope of 0.98 (R^2=0.82). Perfect agreement is not expected due to lack of complete overlap in the measured size ranges, effects on sizing of particle non-sphericity, and since SMPS is measuring a different particle size at each point in space (time), while the AMS does an interleaved average as discussed above. At high mass loadings the AMS is above the fit line, which could be due to ammonium nitrate evaporation in the SMPS (Gysel et al., 2007), which was maintained at 40°C to improve RH control in the tandem differential differential mobility analyzer (TDMA) that was located in the same enclosure as the SMPS.

3.1.3 Calculated scattering vs. measured scattering

Scattering calculated from AMS size-resolved composition was compared to the averaged nephelometer measurements. Figure 2d shows that agreement is good for most of the flights. During flights with lower aerosol concentrations there is more scatter, likely because the AMS size distributions are noisier for low loading (especially for larger sizes) and this noise is amplified with the non-linearity in the scattering calculation. Calculated scattering from INTEX-B was also included in this figure to show the general agreement with MIRAGE and shows the lower loadings sampled during the INTEX-B campaign (Dunlea et al., 2008).

3.2 Submicron Aerosol Chemistry over and away from Mexico City

Bulk NR-PM_1 composition was averaged for the whole aircraft campaign as well as for periods when the aircraft was over Mexico City (defined as the box between 19.814, 19.023 N, and 260.577 and 261.379). Figures 3a–c show this information. Figure 3d shows the average aerosol composition as measured at the ground during the entire campaign at the T0 supersite (19.48973 N, −99.1501 W) at the typical times of day (12:00–18:00 local time) when the C-130 flew over the city. The average for the whole campaign was used for T0 as there were only a few direct flyovers and both instruments were not always operating during those times, and also because the bulk aerosol composition was not highly variable at T0. The relative concentrations of organic and total inorganic species are very similar. The fraction of organics from the MCMA-2003 campaign (Salcedo et al., 2006) is larger than the fraction reported in this study, but this is due to the MCMA-2003 study reporting a full day average. A full day average would increase the mass fraction of organics because there are higher primary organics and lower ammonium nitrate concentrations during evenings, nights, and early mornings.

The spatial and vertical distribution of the species showed significant differences. Figure 3c shows that away from the city the total average concentration is ∼1/4 of that over the city, confirming the importance of the MCMA as a regional source, and with an increased fraction of sulfate at the expense of nitrate. In general, sulfate was more of a regional component to the aerosol with similar concentrations both in the MCMA basin and in the regional airmass, while nitrate was localized to the city and in the near-outflow. This is consistent with the conclusions of Salcedo et al. (2006), who based them on the rapid variability and strong diurnal cycles of nitrate in the city, versus the much more constant and slowly varying levels of sulfate, as well as the fact that $OH+NO_2$ could explain the rapid nitrate increases observed

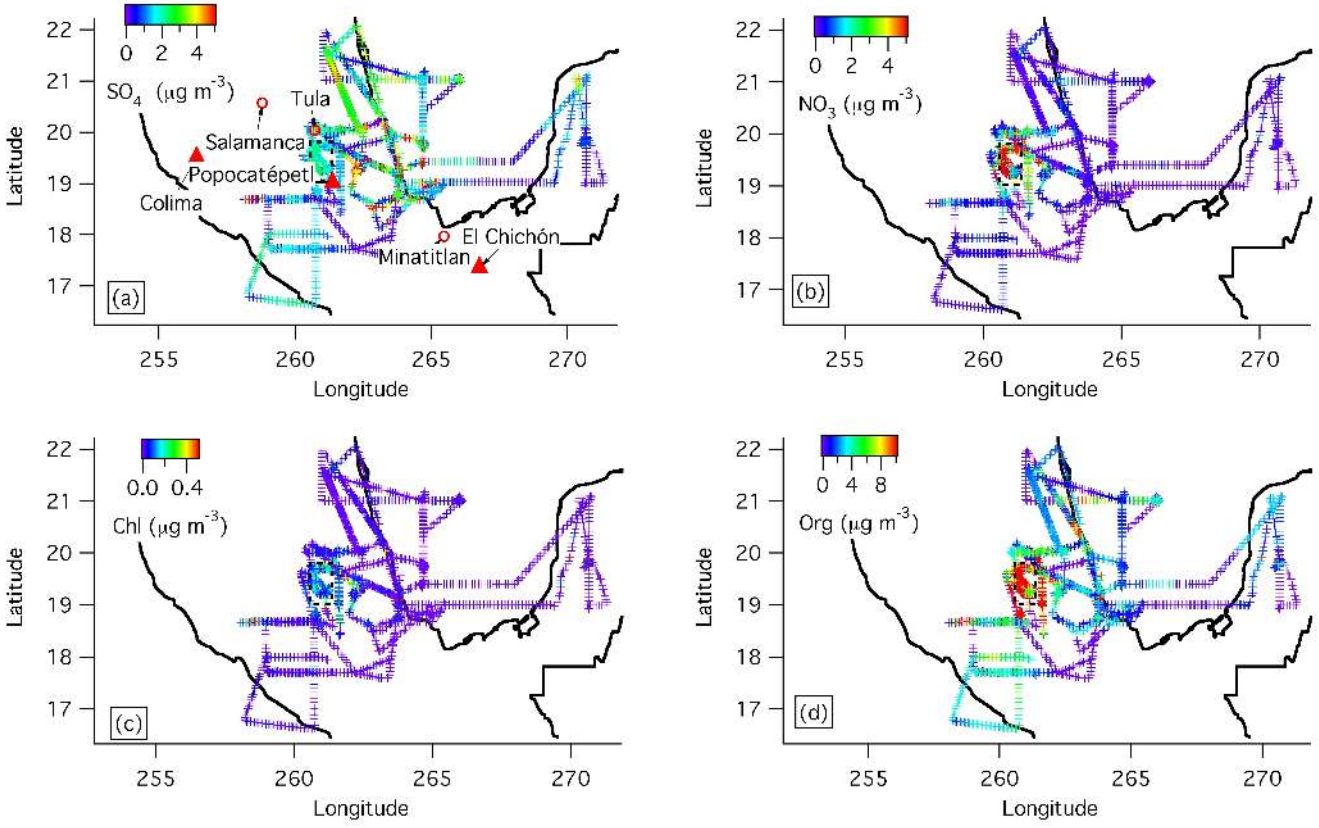

Fig. 4. Spatial maps of **(a)** NR-PM_1 sulfate, **(b)** NR-PM_1 nitrate, **(c)** NR-PM_1 chloride, and **(d)** NR-PM_1 Organics. The dashed box represents the area designated as "city" in Fig. 3. Several large SO_2 sources for the region are indicated in part (b). Volcanoes are designated as red triangles, petrochemical refineries indicated by hollow circles. Both Popocatepétl and Colima were active in 2007, while the last known eruption of El Chichón is 1982 (Smithsonian, 2007). Also note that the colorscale for part (d) is double that of parts (a) and (b), and the scale of part (c) is 10% of parts (a) and (b).

Table 1. Results of the Organic Aerosol to CO regression analysis for RFs 1, 2, 3, 9, 10, 11, 12. RFs 1, 2, 3, 12 had a city and regional component; the rest of the flights are included for completeness, but do not represent the same range of conditions. CO background is given by the X-axis intercept for the low CO (<200 ppbv) conditions. Slopes are the OA/CO ratio for each flight. The R^2 value is given to indicate the quality of fit.

		RF 1	RF 2	RF3	RF9	RF10	RF 11	RF12
	Units (STP)	4 March	08 March	10 March	23 March	26 March	28 March	29 March
OA/CO (low CO)	$\mu g\,m^{-3}$ ppmv^{-1}	77.9	81.1	84.8	62.5	32.5	47.0	80.2
Estimated CO background	ppbv	73.1	78	61	74	63	73	93
R^2		0.84	0.53	0.82	0.65	0.25	0.50	0.78

in the mornings, while sulfate formation from OH+SO_2 was small compared to the concentrations observed. Kleinman et al. (2008) analyzed the increase of the sulfate/CO for their MILAGRO dataset from the G-1 aircraft in the MCMA outflow. However, given the lack of correlation of sulfate with urban pollutants, this analysis may have led to an artificially inflated rate of growth of sulfate/CO for this species in the results of Kleinman et al., as CO decreased due to dilution but sulfate did not due to its more regional character. Spatial maps of NR-PM_1 sulfate, nitrate, and chloride are shown in Fig. 4a-c. Both industrial sources and volcanic sources have been identified as potentially contributing to the aerosol sulfate in the basin (de Foy et al., 2007; Johnson et al., 2006b; Raga et al., 1999; Salcedo et al., 2006). The maps show the more regional distribution of sulfate with significant structure indicating the influence of the large SO_2 sources from industrial complexes (e.g. Tula and refineries near Veracruz) and active volcanoes (e.g. Popocateptl). Emissions of SO_2

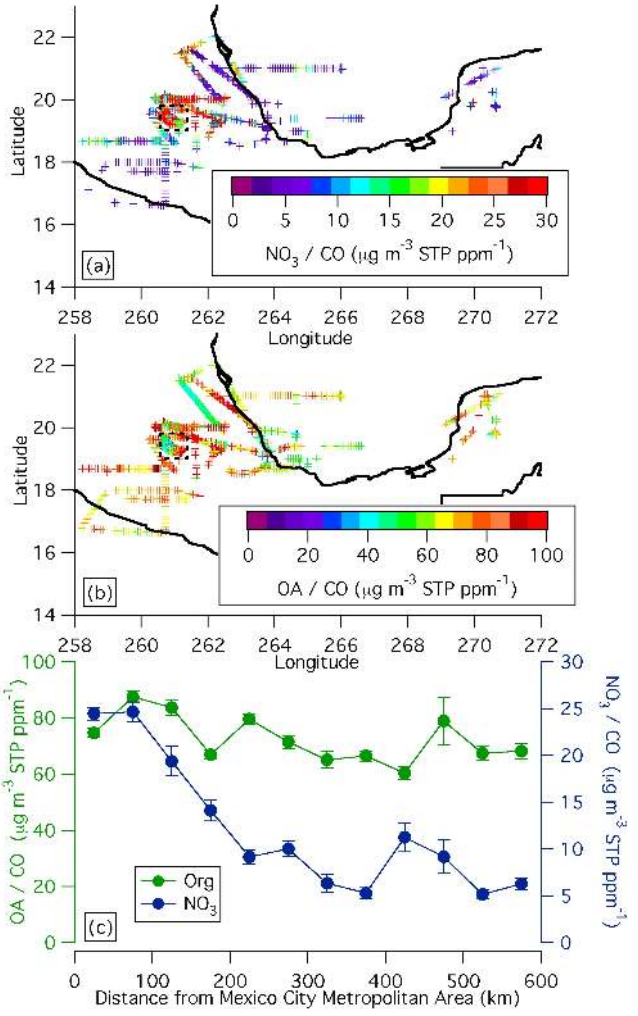

Fig. 5. Shows OA and NO_3^- aerosol components divide by excess CO to account for dilution. Part **(a)** shows a spatial map of the OA/CO ratio. Part **(b)** shows a spatial map of the NR-PM_1 nitrate/CO ratio. Part **(c)** shows the average OA/CO and NO_3/CO ratio as a function of distance from Mexico City. The error bars are the standard error of the mean for all of the measurements in that distance bin. Points from the Yucatan portion of RF 9 were excluded from this analysis due to the influence of local fires from that region.

from Popocateptl were also monitored directly during MILAGRO, when the volcano was a continous source of SO_2 and its emissions varied from a minimum of 0.56 Gg/day to a maximum of 5.97 Gg/day (Grutter et al., 2008). Submicron aerosol nitrate appears to be in the form of ammonium nitrate, based on the ammonium balance and observed fragmentation pattern (see below), while the fractional contribution of organic nitrates to total nitrate appears to be small. Nitrate shows a dominant source in the city basin, and correlates strongly with CO in the city basin (R^2=0.79) but not with HCN (R^2=0.10) indicating the dominance of the urban non-fire source for this species. Mexico City is characterized by high concentrations of gas-phase NH_3 that favor its co-condensation with nitric acid to form semivolatile ammonium nitrate (San Martini et al., 2006). In contrast, fire plumes around Mexico City have a large molar excess of NO_x vs. NH_3 (Yokelson et al., 2007), which may explain the limited ammonium nitrate formation. Nitrate shows a very large fractional reduction in the outflow, most likely due to evaporation upon dilution with regional air with low HNO_3 and NH_3, or the loss of NH_4^+ to sulfuric acid or ammonium bisulfate. Regional temperature gradients do not appear to play a role, as the average temperature measured on the C-130 is approximately 5°C higher above the city box than the regional air, which would favor evaporation in the city and condensation away from the city. HNO_3 also reacts with dust in the Mexico City area forming mineral nitrates in the supermicron mode (Fountoukis et al., 2007; Moffet et al., 2007; Querol et al., 2008) that would not be detected by the AMS. However the dust spatial and temporal distribution is highly variable and is unlikely to be the only cause of the pronounced decrease in nitrate away from the city observed in this study. Figures 5a–c show the ratio of organic and nitrate aerosol to excess CO to remove the effect of dilution in the cleaner regional air. Excess CO is defined as the CO concentration above background, with the background value for each flight given in Table 1. Additionally data with OA concentrations less than 2 μg m^{-3} STP or NO_3 concentrations less than 0.2 μg m^{-3} STP were eliminated from the analysis to reduce the impact of noise and of uncertainty in the CO background (90% of the points used in the analysis had CO excess >35 ppbv). Clearly NO_3/CO shows a large reduction with distance from the Mexico City urban area, while OA/CO does not. Although aerosol nitrate does not completely disappear, its ratio to CO decreases quickly and has dropped by nearly a factor of 4 by the time the aircraft is 200 km from the city basin. The OA/CO ratio in the outflow near the city is about 80 μg m^{-3} STP ppm^{-1}. This is likely due to a combination of rapid SOA formation from urban emissions and mixing of biomass burning OA, and will be analyzed in more detail in a subsequent publication. This ratio is similar to the value found by Kleinman et al. (2008), for their study of the near outflow on the DOE G-1 aircraft. It is also much larger than values of 5–10 μg m^{-3} STP ppm^{-1} for urban POA (Aiken et al., 2007a; Zhang et al., 2005c), which highlights the dominance of SOA in the pollution outflow of the city, consistent with previous observations in Mexico City (Kleinman et al., 2008; Volkamer et al., 2006, 2007) and at several other locations (Zhang et al., 2007a). Both the asymptotic value of OA/CO and the timescale of SOA formation of approximately one day are similar to findings reported for the outflow of the Northeastern US (de Gouw et al., 2005, 2008; Kleinman et al., 2007; Peltier et al., 2007a), and of the Po Valley in Italy (Crosier et al., 2007). The fact that similar asymptotic values are observed despite lower biogenic emissions being added to anthropogenic pollution

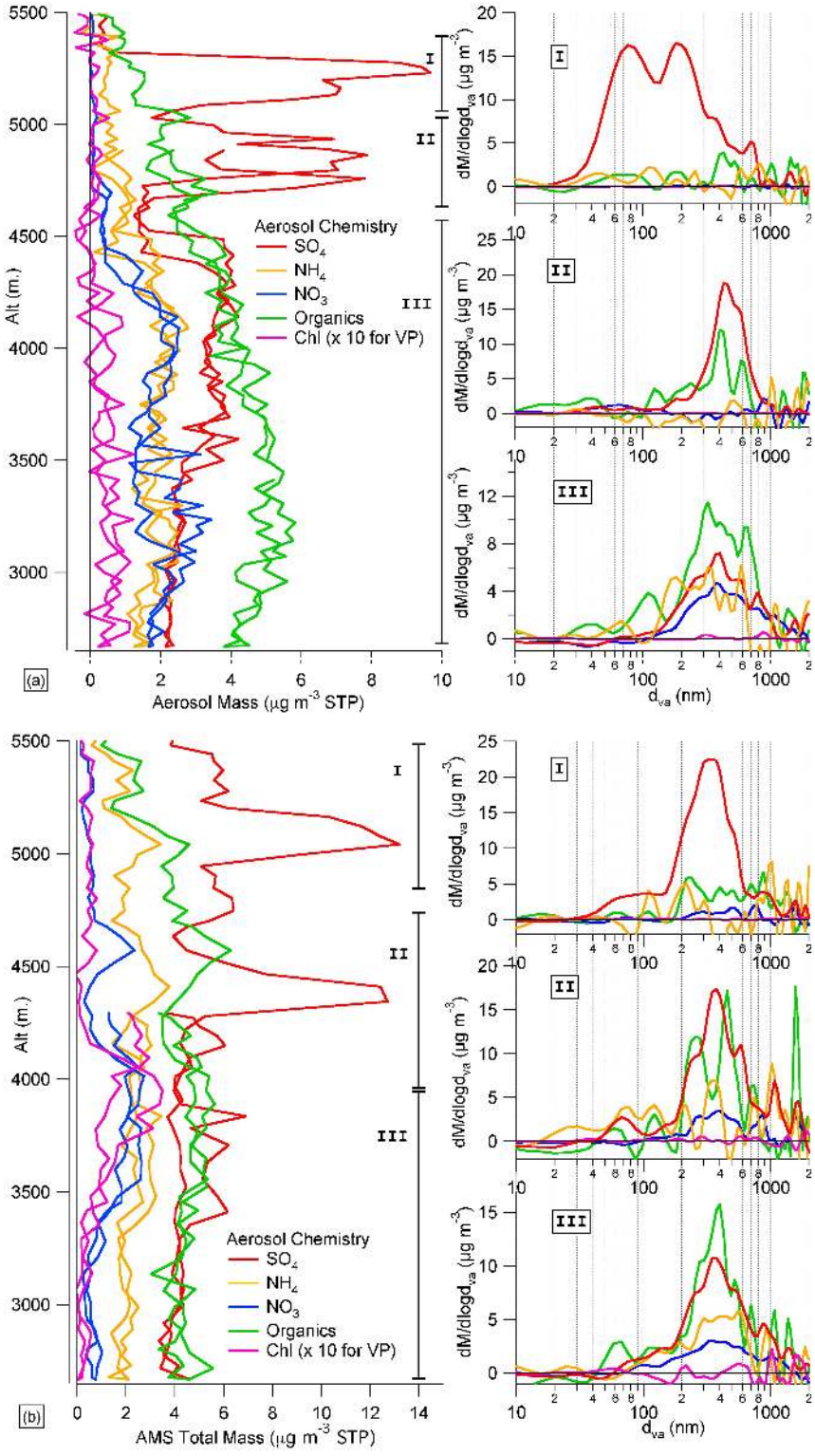

Fig. 6. Vertical profiles east of the Popocatepetl volcano for 2 different times during Research Flight 12. For both profiles the lowest point corresponds to an altitude ∼300 m above the ground, and the locations of the profiles are shown in Figure S-1 in the supp. info. The first profile took place from 17:34–18:02 UTC at 19.29 N and −97.63 W. The second profile took place from 21:02–21:19 UTC at 19.23 N and −97.8 W. Two elevated acidic sulfate layers are clearly seen on both profiles. See text for further description.

during MILAGRO versus the summer in New England could be due to the higher BB emissions in Mexico during this study (Yokelson et al., 2007; Stone et al., 2008).

NR-Chloride shows sources both in and outside of the Mexico City basin. Often the NR-Chloride is associated with HCN indicating a fire source, however there are instances of chloride plumes without an associated increase in HCN, indicating other sources as well, consistent with previous results (Salcedo et al., 2006) and studies at other locations (Tanaka et al., 2003). The nitrate fraction showed an enhancement in the aircraft data at altitudes less than 2 km as compared with the ground data qualitatively consistent with previous studies (Morino et al., 2006; Neuman et al., 2003) likely due to additional ammonium nitrate condensation with lower temperature and higher relative humidity aloft, whereas the average mass fraction of aerosol sulfate at the T0 ground site was higher than it was aloft over the city basin measured by the C-130 during the MIRAGE campaign.

Figure 6 shows two vertical profiles performed outside of the city basin to the east of the Popocatepetl volcano during RF 12 (29 March 2006). The detailed locations are shown in Fig. S-1 in the supplementary information (http://www.atmos-chem-phys.net/8/4027/2008/acp-8-4027-2008-supplement.pdf). During the first vertical profile (17:30–18:00 UTC) 2 acidic sulfate layers are seen at high altitude, which have increased in vertical separation later in the flight when a second vertical profile (21:00–21:20 UTC) was made in the same area. Size distributions for the parts of the vertical profile marked I, II, and III are shown to the right of the vertical profile. The first vertical profile shows that the highest sulfate layer (I) has small aerosol size modes of highly acidic sulfate most likely from recent nucleation and growth in the volcanic plume, similar to the nucleation and growth study of Zhang et al. (2004). The second, sulfate layer (II), lower in altitude, consists of larger particles, indicating a more aged layer but still very acidic, and the lowest layer (III) extending to the bottom of the profile contains a mix of organics, ammonium sulfate and ammonium nitrate is likely pollution transported from the Puebla basin based on back trajectories. The second vertical profile performed 3.5 h later indicates that the most of the particles in the highest layer (I) have grown to or coagulated with accumulation mode sizes and increased the sulfate mass loading. This could be due to the additional daylight processing time assuming similar transport times. However there is still a significant tail of mass at particle sizes less than 100 nm. The other 2 size distributions related to layers II and III have not changed significantly during that time. No enhancement of organics is found in the acidic sulfate layers, consistent with other recent field studies that find no evidence for significant acid-catalyzed SOA formation in the atmosphere (Peltier et al., 2007b; Zhang et al., 2007b), although this may also be due to lack of gas-phase SOA precursors in these layers. This case study demonstrates the vertical heterogeneity of the aerosol composition, as well as the high signal-to-noise of the HR-ToF-AMS in the V MS mode, and the ability of the instrument to rapidly determine meaningful chemically-resolved size distributions.

The charge balance of ammonium to inorganic anions (sulfate, nitrate, chloride) can be used to evaluate the acidity or neutralization of the aerosol as long as the contribution of mineral cations (Ca^+, K^+ etc.) is small (Zhang et al., 2007b). This balance is shown in Fig. 7. Large relative concentrations of supermicron volume to submicron volume can influence submicron ion balance due to tailing of the supermicron size distribution (and associate mineral cations) into the submicron. A comparison of the supermicron volume (likely dominated by mineral dust) and submicron volume from the OPC indicate that with the exception of a few short plumes submicron volume was typically a factor of 2 or more larger than supermicron volume. Assuming a dust size distribution similar to those from Maring et al. (2003), this implies that only a few percent of the submicron volume would be due to dust, which is consistent with previous observations in Mexico City (Salcedo et al., 2006) and with measurements at T0 during MILAGRO (Aiken et al., 2007a). This suggests that the contribution of mineral cations to the charge balance due to the submicron tail of the dust mode was small. Charge balance is observed within the scatter for most datapoints, which indicates that ammonium nitrate and sulfate are the predominant forms of nitrate and sulfate in the submicron aerosol. There are, however, instances of highly acidic sulfate plumes originating in some instances from the Popocatepetl volcano (as shown in Fig. 6) and in other instances from petrochemical or power plant complexes such as Tula.

3.3 O/C atomic ratios and OM/OC ratios of organic aerosol

O/C atomic ratios and OM/OC ratios for the total organic aerosol were calculated from the HR spectra with the procedure described by Aiken et al. (2007b; 2008). Figure 8 shows flight tracks for RFs 1, 2, 3, 11, and 12 colored by the organic O/C ratio. This figure clearly shows an increase in the O/C ratio away from the city, with maximum values around ~0.9. The range of values observed for OM/OC is 1.6–2.3, with the lower values corresponding to air over the city and the larger ones to aged regional air. It is also important to notice that even above Mexico City the O/C ratio is already ~0.4 and above, which already represents a highly oxygenated aerosol. This is likely due to flights through the mixed layer above city occurring in the early to late afternoon when photochemical SOA formation has already been active for hours (Kleinman et al., 2008; Salcedo et al., 2006; Volkamer et al., 2006), as well as to BB influence (see below). Primary urban emissions from vehicles have much lower O/C ratios around 0.06-0.1 (Aiken et al., 2008). This indicates that a significant amount of secondary formation has already occurred by the time the C-130 reaches the city.

The influence of BB on the organic O/C ratio is investigated in Figure 9 by plotting HCN vs O/C ratio for RF3

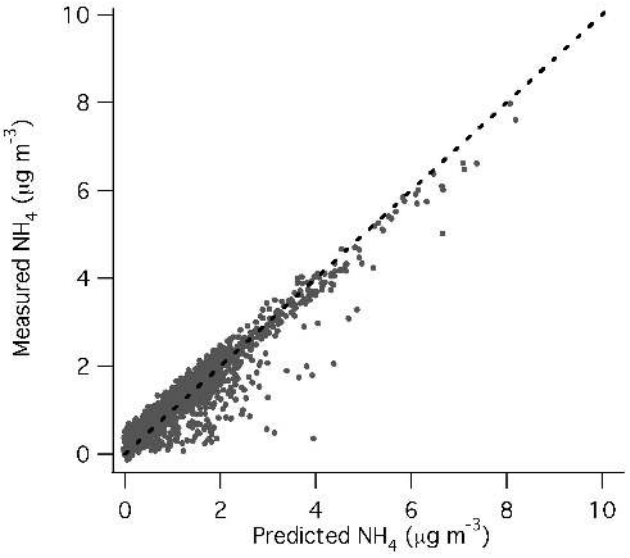

Fig. 7. Scatter plot of measured ammonium versus the amount needed to fully neutralize the measured submicron nitrate, sulfate, and chloride. Dashed line is the 1:1 line. Points below the line are nominally acidic, while points above the line are nominally basic.

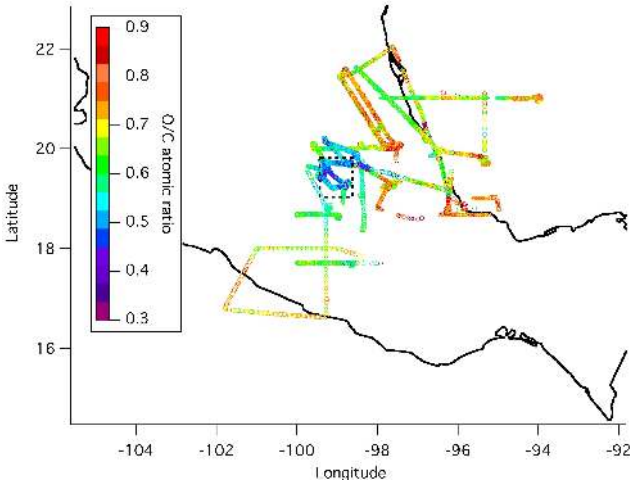

Fig. 8. Flight tracks for RFs 1, 2, 3, 11, and 12 colored by the organic O/C atomic ratio. RFs 9 and 10 were excluded from this plot since there was no city component of these flights. Only data points with OA concentrations greater than $2\,\mu g\,m^{-3}$ are shown, to reduce the effect of noise on the O/C calculation. The organic aerosol is clearly more oxidized away from the dominant source in the region, the Mexico City basin. Box indicates the Mexico City urban area.

(10 March 2006) which included high concentrations of BB aerosol over the Mexico City basin. Using a concentration of 1000 pptv or greater of HCN as an indicator of fresh BB plumes, the O/C range for primary biomass burning OA (P-BBOA) is estimated as 0.3–0.45, which are similar to the values observed in laboratory BB experiments (Aiken et al., 2008; Huffman et al., 2008a[3]). The range of values may be due to both residence time in the atmosphere (SOA formation, oxidation, and/or volatile evaporation due to dilution) and/or inherent variability in biomass burning plumes from differences in the vegetation burned and fire conditions (e.g. smoldering vs. flaming). Only a few plumes were sampled, consequently the range of values may be broader than what is given here, but this is useful as an indicator of approximate O/C ratios for biomass burning.

From Fig. 8 it is clear that organic O/C ratios increase significantly away from the city, with distance being a proxy for the age of the aerosol; i.e. aerosol outside the city can have a city origin and have been aged during transport, or a regional non-city origin. Regional air typically shows aged characteristics due to the longer average residence time of the OA sampled in the regional air (Zhang et al., 2005b, 2005c). Since thermodynamics drives atmospheric organics towards increased oxidation, the increase in the organic O/C ratio is indicative of aging of the aerosol, and in the absence

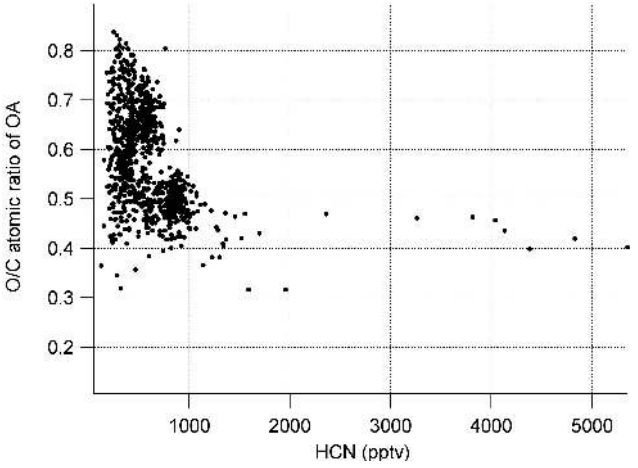

Fig. 9. O/C atomic ratio for OA vs HCN for RF 3 10 March 2006. Intense fire plumes are indicated by HCN concentrations exceeding 1000 pptv, and show an O/C ratio of BBOA ranging between 0.3 and 0.45.

of calibration or kinetic modeling, it is a qualitative indicator of photochemical age. Recent results by Huffman et al. (2008a)[3] indicate that SOA in Mexico City is less volatile than urban POA and most P-BBOA, so some of the increase in the O/C ratio in the regional scale may be due to evaporation losses of more reduced species. This is likely not the dominant effect since primary O/C ratios are low for urban combustion emissions, and around 0.4 for biomass burning plumes, and to reach O/C ratios of 0.6–0.8, addition of

[3]Huffman, J. A., Aiken, A. C., Docherty, K. S., Ulbrich, I. M., DeCarlo, P. F., Jayne, J. T., Onasch, T. B., Trimborn, A., Worsnop, D. R., Ziemann, P. J., and Jimenez, J. L.: Volatility of primary and secondary organic aerosols in the field contradicts current model representations, Environ. Sci. Technol., submitted, 2008a.

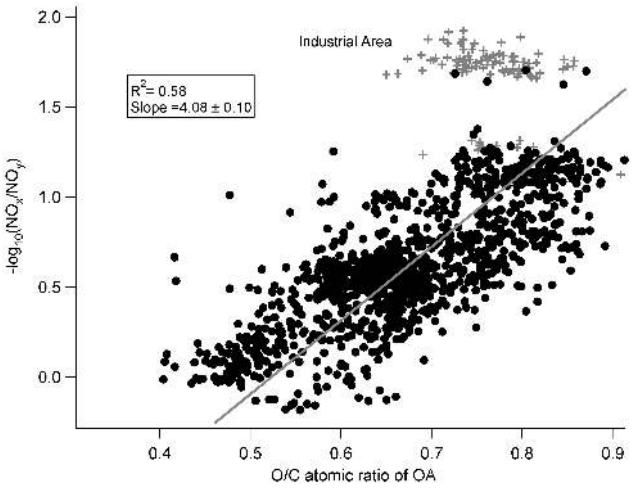

Fig. 10. Relationship between $-\log_{10}(NO_x/NO_y)$ and O/C atomic ratio of organic aerosols during RF12 (29 March 2006). Clear correlation between these 2 indicates that O/C of OA increases with photochemical age. Data points marked with crosses are likely impacted by aged petrochemical emissions and are not representative of urban outflow and are excluded from the fit.

SOA of higher O/C ratios, or heterogeneous oxidation of the aerosol need to occur. However, heterogeneous oxidation of the emitted primary aerosols cannot explain the large mass of SOA rapidly formed. Also, heterogeneous oxidation proceeds with longer timescales of the order of 1 week or longer (Molina et al., 2004; Murphy et al., 2007; Schauer et al., 1996; Zhang et al., 2005a). An order-of-magnitude calculation (see Appendix 1) comparing the gain of O observed in Fig. 8 vs. an upper limit of what could be expected from OH heterogeneous oxidation shows that heterogeneous oxidation is expected to be too slow by a factor of ∼7–135 to explain the rate of O increase observed here, i.e. only ∼0.7–14% of the increase in O/C can be explained by heterogeneous reactions. This is consistent with the results of the only study of heterogeneous aging on ambient particles to date (George et al., 2008), which observed a gain of O/C (estimated from their results and the correlation of m/z 44/OA and O/C of Aiken et al. (2008)) about 11 times slower than than observed here. As SOA formation has a timescale around 1 day (de Gouw et al., 2005; Peltier et al., 2007a), additional SOA formation (from urban and BB precursors) or additional gas-phase oxidation of semivolatile SOA species are the most likely reasons for the observed increase in O/C. Downwind of the city basin the increase in the O/C ratio while OA/CO stays approximately constant implies that there is a loss of organic carbon from the OA (e.g. by evaporation upon dilution), since the addition of oxygen to the OA without subsequent loss of organic carbon would increase the OA/CO ratio, but this is not observed. Significant loss of carbon due to heterogeneous reactions is unlikely, given the constraint provided by Murphy et al. (2007). These authors observed the timescale of this process to be of the order of several months for tropospheric accumulation mode particles (dominated by sulfate and organics, very likely OOA) in the lower stratosphere despite high oxidant levels. High rates of carbon loss due to heterogeneous reactions have only been reported in the laboratory for very reduced particle compositions which are not representative of atmospheric OOA (e.g. Molina et al., 2004) and were only observed for equivalent aging times longer than 9 days when oxidizing ambient particles in the laboratory (George et al., 2008).

Another qualitative measure of photochemical age is the $-\log_{10}(NO_x/NO_y)$ ratio (Kleinman et al., 2007). This and other such ratios work best if there is an isolated source or source region, which does not mix with other sources from emission to the time of sampling. This can be a problem when using this ratio when urban pollution mixes with fire plumes, as fire plumes from the pine forests near Mexico City had high NO_x emissions (Yokelson et al., 2007). When air from different sources mixes this photochemical clock is "reset" losing information on the age of pollution from both sources. For this reason we compared the organic O/C atomic ratio to the $-\log_{10}(NO_x/NO_y)$ from RF 12 (29 March 2006), when biomass burning was low, and gas phase data of HCN and CO did not indicate recent biomass burning influence. Figure 10 shows a comparison between the $-\log_{10}(NO_x/NO_y)$ ratio and the O/C ratio. There is a clear trend which shows the increase in the $-\log_{10}(NO_x/NO_y)$ ratio with increasing O/C ratio, indicating that this is a good qualitative clock for photochemical age. The x-intercept of the regression occurs at approximately an O/C ratio of 0.52. The lowest values of the O/C ratio were found at altitudes of ∼2900 m (a.s.l.) during a transect through the Mexico City basin around 20:20 UTC (14:30 local), which was clearly dominated by pollution sources. The reason for this high value is potentially due to the C-130 arrival into the city in the mid afternoon, by which time a significant fraction of the total SOA formation has already occurred. The $-\log_{10}(NO_x/NO_y)$ clock can also be "reset" by mixing fresh high NO_x plumes with older pollution. Since secondary OA mass rapidly exceeds primary OA the mixing of a fresh plume with low concentrations of OA (and low O/C) would only minimally affect the O/C ratio which would be dominated by the higher O/C ratio of the secondary OA. The group of points above the value of 1.5 for $-\log_{10}(NO_x/NO_y)$ come from a leg of the flight at 18.67 N from 95.88 to 95.16 W longitude, just inland from the Gulf of Mexico and in the vicinity of petrochemical refineries and processing facilities. It is likely that the relationship of $-\log_{10}(NO_x/NO_y)$ to O/C atomic ratio for this section of the flight is more indicative of an aged industrial plume than an urban plume.

3.4 Case study: research flight 2, 8 March 2006

RF 2 provides the opportunity to combine the analysis techniques discussed above into a detailed picture of the

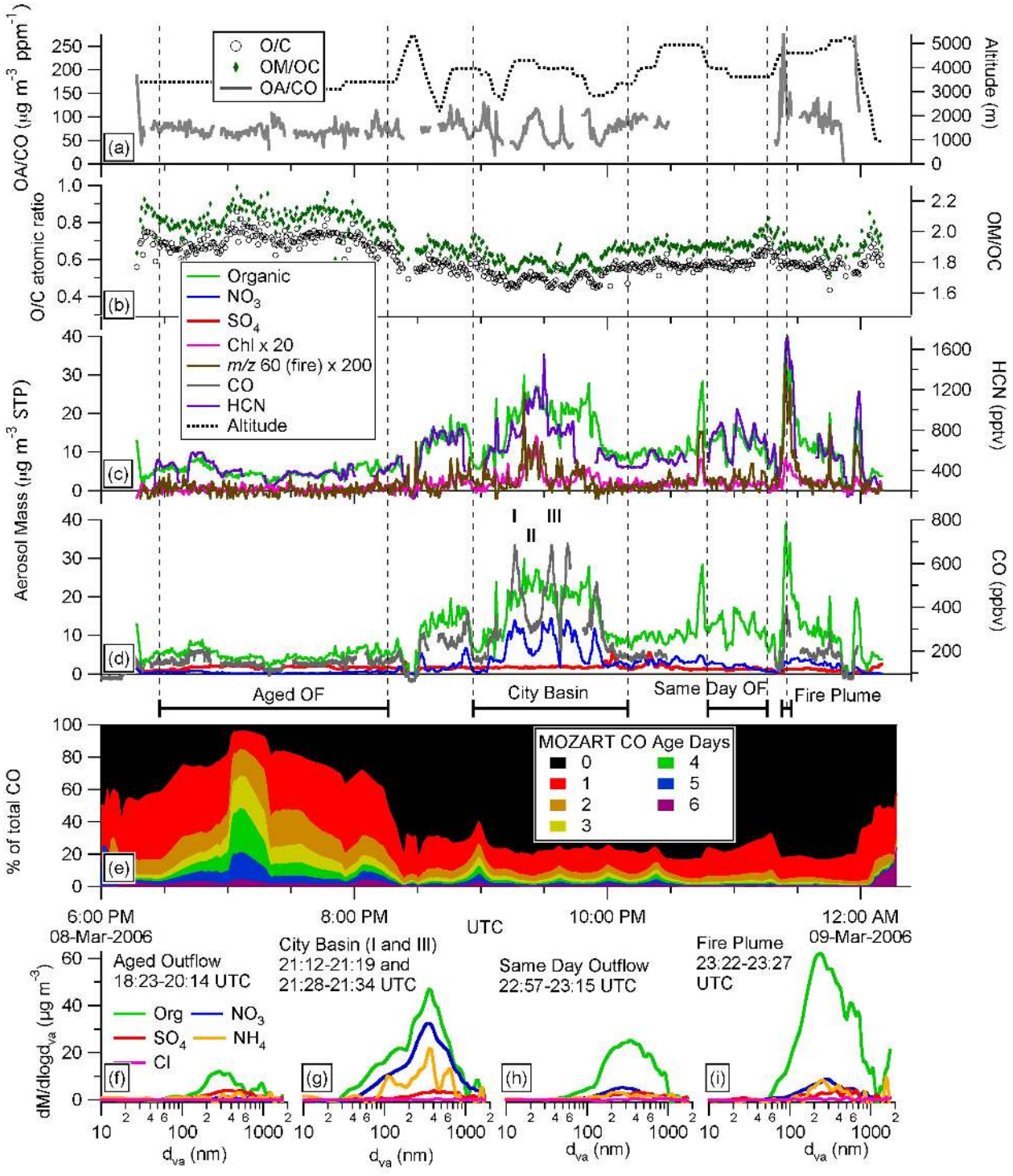

Fig. 11. Time traces of different pollutants and ratios for RF 2 (8 March 2006) Part **(a)** shows the OA/CO ratio, and aircraft altitude. Part **(b)** shows the O/C atomic ratio and OM/OC ratio. Part **(c)** shows time traces of NR-PM_1 Organic and Chloride aerosol with the fire contribution of m/z 60 calculated as: m/z 60–0.003*Organic (see text for explanation), and gas phase HCN. Part **(d)** shows timetraces of NR-PM_1 Organic and Nitrate in the aerosol phase and CO in the gas phase. Periods marked I and III show times when the aerosol was dominated by urban pollution, and period II indicates a time when the aerosol was heavily influence by fire emissions. Part **(e)** shows the contribution in percent of CO emitted from sources in Mexico City based on the emissions and transport from the MOZART model for the flight day and each of the previous 6 days. Parts **(f)–(i)** show size distributions for different parts of the flight as labeled on the figures. All size distributions were subject to 2 point binomial smoothing to reduce high-frequency noise.

aerosol for this flight. AMS sampling for this flight began 1 h into the flight (18:00 UTC or 12:00 local) due to pump down requirements after lack of ground power. The flight consisted of 3 general sampling regimes, which are illustrated in Fig. SI-2 in the supplementary information (http://www.atmos-chem-phys.net/8/4027/2008/acp-8-4027-2008-supplement.pdf). The first regime sampled aged outflow from the previous day southwest of the city basin where the forecast models predicted it to be located. The second portion of the flight involved a standard city flight pattern with the C-130 entering the city basin from the northwest and flying south along the western edge of the basin. The aircraft then turned east and flew along the southern edge of the basin, turning around in the southeast corner of the basin and flying northwest across the city. A pass over the T0 supersite and stacked legs over the T1 supersite were then performed. The final portion of the flight consisted of stacked legs to the east of the city basin sampling same day pollution which had been advected to that vicinity based on the meteorological predictions.

Figure 11 shows the time traces of many pollutants and properties of the pollutants, and is discussed in detail in the following text. Figure 11e shows the day tagged CO emissions from the MOZART model, and qualitatively indicates the age of the sampled air mass. Early in the flight the air mass is clearly more aged than the latter portion of the flight, and is generally characterized by lower aerosol loadings dominated by organics with sulfate as the dominant inorganic component (Fig. 11c and d), with the highest aerosol O/C atomic ratios (up to 0.8) and OM/OC ratios (around 2.1) of any portion of the flight (Fig. 11b). The average size distribution for this portion of the flight shows the mass diameter peaking around 300 nm d_{va} for organics and slightly larger at 400 nm d_{va} for ammonium sulfate, which is the dominant inorganic component. The ammonium size distributions shown in Fig. 11f–i, are noisy due to the water background in the mass spectrometer resulting from limited pumping time, but are shown for completeness. The OA/CO ratio for the first portion of the flight (Fig. 11a) averages 70 μg m^{-3} STP ppmv^{-1} with a standard deviation of +/−11 μg m^{-3} STP ppmv^{-1}.

As the C-130 enters the city basin around 21:00 UTC (03:00 PM local time), the CO age from the MOZART model indicates that ∼80% of the CO is from the same day emissions (Fig. 11e). Aerosol nitrate becomes the dominant inorganic aerosol component, with organic aerosol still dominating the submicron mass (Fig. 11c and d). The organic O/C atomic ratio and OM/OC ratio reach the lowest values for the flight (approximately 0.5 and 1.7 respectively). Size distributions show organics and ammonium nitrate peaking at 350 nm d_{va}. Sulfate is a minor component of the aerosol, but shows a slightly higher mass diameter around 450 nm d_{va} indicative of its more aged and regional character (Fig. 11g). The OA/CO ratios (Fig. 11a) are highly variable indicating the influence of fire emissions on the aerosol. Lower values of approximately 40 μg m^{-3} STP ppmv^{-1} CO are reached during the periods marked I and III in Fig. 11d. These periods are associated with high CO, high aerosol nitrate, and are indicative of "fresh" urban SOA. The period marked II in Fig. 11d has a higher OA/CO ratio averaging 100 μg m^{-3} STP ppmv^{-1} CO, and is associated with high levels of HCN, and NR-aerosol chloride. AMS m/z 60 is used as a marker for biomass burning (Alfarra et al., 2007; Schneider et al., 2006), however, it is not completely unique to fire emissions, and during non-fire periods m/z 60 makes up approximately 0.3% of the organic mass, consistent with SOA chamber spectra (Ulbrich et al., 2008). By subtracting 0.3% of the organic mass from m/z 60 we have a good indication of the fire contribution to signal at this m/z. This scaled m/z 60 also increased during period II, adding yet another indication of the influence of a fire source. This marker appears to be a good tracer for fresh fire plumes during this study. Although it is possible that this marker is partially lost due to volatilization (Huffman et al., 2008a[3]) and/or photochemical reactions with aging, recent field results indicate that its lifetime is of at least two days (Lee et al., 2008; and our own results during the 2008 NASA ARCTAS field campaign). Finally during period II, the presence of ∼5 μg m^{-3} STP of ammonium nitrate indicates that there is still a large urban influence in this plume.

Figure 12a shows the mass spectrum for the period I. This mass spectrum is very similar to observed organic spectra from other urban locations (Alfarra et al., 2004; Docherty et al., 2008; Zhang et al., 2005c). A comparison of the fractional contribution of each m/z to the total organic signal using the procedure of Alfarra et al. (2006), shows differences in the spectra from periods I and II and the similarity for periods I and III (Fig. 12b and c). When comparing the relatively fresh fire-dominated period (II) with the urban-dominated period I, only a few peaks below m/z 120 have a higher percent contribution to the aerosol mass. The most pronounced ions that are larger in BB plumes are m/z 60 and 73, which are found in the mass spectra of levoglucosan (a component of biomass burning aerosol), and have been shown to be marker peaks for biomass burning in ambient air (Alfarra et al., 2007; Schneider et al., 2006). Although not shown the same pattern emerges when comparing period II with period III. Figure 12c demonstrates the similarity between periods I and III with very little change in the relative contributions for the mass spectra. Deviations from the 0% change in contribution are mostly due to noise at m/z with low S/N. Also clear from this plot is the increase in the contribution to organic mass of high m/z (above m/z 120) for biomass burning. While the majority of the signal in all cases (I-III) is below m/z 100 (91.4%, 90.6%, 91.5%, for Cases I-III, respectively) this indicates that biomass burning plumes contain either larger molecules, or molecules more resistant to fragmentation than those in urban POA and SOA.

The final portion of the flight showed increases in the O/C atomic ratio and OM/OC ratio compared to the city

(Fig. 11b), but these variables did not increase to the levels seen in the aged outflow from the early part of the flight, consistent with the lower average age of the air predicted by MOZART. This part of the flight also included some advected fire plumes indicated by increases in the OA/CO ratio (up to 250 μg m^{-3}STP ppmv^{-1}), HCN, NR-chloride, and m/z 60 (Fig. 11b and c). Size distributions for the period marked same day outflow (OF), and fire plume are shown in Fig. 11h and i. The same day outflow size distribution shows a clear drop in aerosol nitrate from the city plume, reduced importance of ultrafine particles below 100 nm, and a peak in the distribution at 300 nm d_{va}. The fire plume distribution shows the clear dominance of organics in the fire plume, and the presence of nitrate in the size distribution suggests that the fire plume is adding to the urban pollution, although some of the nitrate may also originate from fire emissions. The mass size distribution for the fire plume peaks at a slightly smaller size of 250 nm d_{va}.

4 Conclusions

A HR-ToF-AMS was flown for the first time during the MILAGRO campaign. The performance of the instrument was very good, providing 12-s quantitative aerosol size and chemistry data. Comparisons between submicron volume from a SMPS, and light scattering confirm the quantification of the AMS data. Organic species dominated the submicron aerosol both near the source and in the outflow and regional air. Inorganic components also made a large contribution, with different species showing different spatial characteristics. Aerosol sulfate had a more regional but still somewhat structured character with clear volcanic and petrochemical/power plant sources. Submicron nitrate showed a strong city source and a high correlation with CO that links it to urban emissions. The higher source strength of NH_3 in the city versus the fires may explain the preferential formation of nitrate in city air, given the comparable NO_x emissions of both sources. Ammonium was associated with nitrate and sulfate, indicating the dominant forms of these species were ammonium nitrate and ammonium sulfate respectively. NR-aerosol chloride was often associated with HCN indicating a fire source, although some chloride plumes did not show this correlation, indicating other sources of NR chloride. Organic aerosol had strong correlations with both CO and HCN indicating both urban and biomass burning sources. The organic O/C atomic ratio showed more reduced aerosol near the city/source regions and higher values farther from the city. O/C was also shown to be a qualitative photochemical clock by comparison to –$\log_{10}$(NO_x/NO_y). SOA formation from urban sources quickly overwhelms urban POA emissions as shown by the increase of the O/C ratio to values much larger than those of urban POA, and consistent with the results of Volkamer et al. (2006) and Kleinman et al. (2008). A case study of the 8-March-06 research flight illustrates the

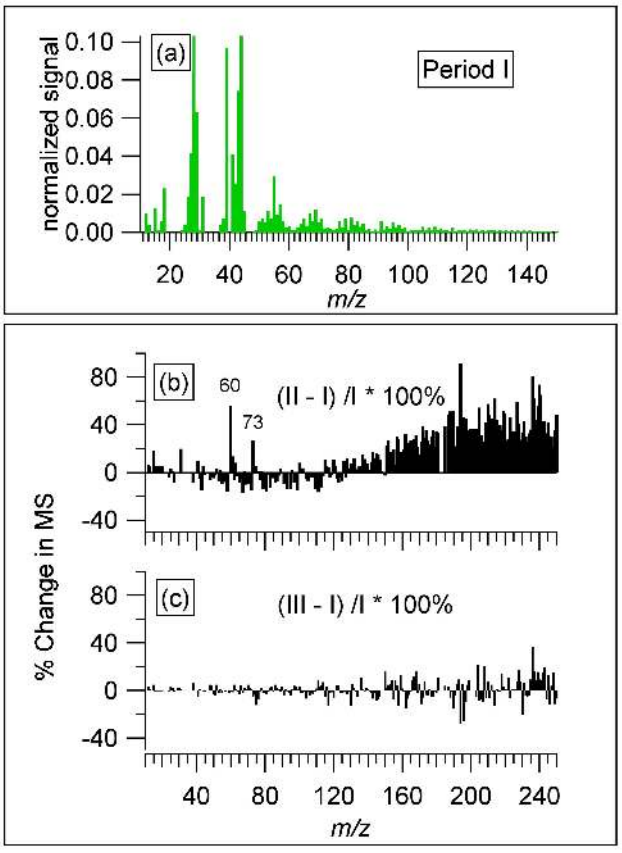

Fig. 12. Part **(a)** shows the organic mass spectrum for the period marked I in Fig. 11. Part **(b)** shows the percent change in contribution to the total organic signal between the biomass and urban-dominated cases, I and II. Part **(c)** shows the percentage change between the 2 urban-dominated periods I and III. The minimal change here indicates the similarity between these 2 periods. The procedure for this plot follows Alfarra et al. (2006): each mass spectrum is normalized to sum to 1. Then the difference in signal for each ion of 2 spectra is calculated, and then divided by one of the spectra and displayed as a percentage.

conclusions above, and indicates that in the AMS mass spectra of BBOA the larger m/z fragments are enhanced, and that m/z 60 and m/z 73 are good marker peaks for biomass burning aerosol in this study.

Appendix A

This appendix details the calculation of the estimated uptake of oxygen by the organic aerosol during photochemical aging (Fig. 10) by heterogeneous reactions, and compares it to the experimentally observed gain of oxygen.

The mode of the organic aerosol mass distribution is chosen as the typical size. Smaller particles would gain oxygen

faster while larger particles would gain oxygen more slowly than in the calculation shown here. Using the peak of the mass distribution from Figs. 6 and 11 in vacuum aerodynamic diameter (d_{va}, measured by the AMS), assuming particle sphericity, and estimating the average material density (ρ_p) from the measured AMS components (DeCarlo et al., 2004), we find a volume equivalent diameter (d_{ve}) of 230 nm.

The organic mass (OM) of a particle of this size can be calculated using Eq. A1:

$$OM = \frac{\pi}{6} d_{ve}^3 \rho_p MF_{\text{org}} \tag{A1}$$

where MF_{org} is the mass fraction of organics species in the particle. Assuming 60% for the mass fraction of the organics from Figure 3, and an estimated ρ_p of 1.43 g cm^{-3} (see Sect. 2), the OM of the assumed particle is 5.45×10^{-18} kg (i.e. 5.45 fg). Assuming that the organic mass and size of this particle remains constant during aging, the mass of oxygen in all of the organic species in the particle (O_{mass}) can be calculated using Eq. A2:

$$O_{\text{mass}} = \frac{OM}{OM/OC} \cdot O/C \cdot \frac{16}{12} \tag{A2}$$

where OM/OC is the Organic-Mass-to-Organic-Carbon ratio, O/C is the atomic oxygen to carbon ratio (both estimated from the high-resolution AMS data), and 16/12 is used to convert the O/C atomic ratio into an O/C mass ratio. Using the O/C atomic ratios of 0.55 and 0.85 from Fig. 8, and the corresponding OM/OC ratios of 1.87 and 2.25, respectively (Aiken et al., 2008), the oxygen mass in the particle at the beginning is 2.13×10^{-18} kg and increases to 2.74×10^{-18} kg. This indicates a gain of 6.10×10^{-19} kg of oxygen in the particle, or 2.30×10^{7} atoms of oxygen during this aging process.

The uptake of oxygen by heterogeneous reaction can be estimated assuming an uptake coefficient (γ) due to reaction with OH. γ=1 is used as an upper limit. However γ is likely lower for highly oxygenated OA with an O/C ratio >0.55 so the calculations are also carried out with γ=0.1. The estimated 24-h average OH concentration around Mexico City is 1.46×10^{6} (C. Cantrell, NCAR, personal communication, 2008). From kinetic theory the average molecular speed of OH speed, $\bar{c}$, is 600 m s^{-1}. A correction factor, α, of 0.9 is used to account for the diffusion limitation to mass transfer, assuming a pressure of 0.5 atm (Seinfeld and Pandis, 1998, Fig. 11.2). The number of OH collisions with the particle surface, C_{OH}, can then be estimated as:

$$C_{OH} = \alpha \frac{\gamma \bar{c}}{4} \cdot \pi d_{ve}^2 [OH] \Delta t \tag{A3}$$

where Δt is the aging time of 24 h, estimated from the change in the $-\log(NO_x/NO_y)$ ratio from Fig. 8. The result of the calculation is 2.82×10^{6} collisions with OH. We assume that the surface is 60% organic (same as the mass fraction) which results in 1.69×10^{6} collisions of OH with an organic molecule a the surface. If it is assumed that each successful collision results in the addition of between 1 and 2 oxygen atoms to the aerosol organic material, then a γ of 1 implies the uptake of $1.69–3.39\times10^{6}$ O atoms in a 24 h period. A γ of 0.1 implies the uptake of $1.69–3.39\times10^{5}$ oxygen atoms in 24 h. These values range between 7 and 135 times too small to explain the increase in oxygen content calculated from the increased O/C ratio over the same 24 h time period.

Acknowledgements. We are grateful to the NCAR RAF and C-130 personnel for much help and guidance during integration and research flights, especially A. Schanot, P. Romashkin, and M. Lord. We thank R. Bahreini, C. Simmons, and A. Middlebrook of NOAA for help with integration and the PCI. We thank C. Brock of NOAA for providing Mie Scattering code in the Igor programming language. We are also grateful to the rest of the C-130 investigators and the Jimenez group for many helpful discussions. This study was supported by grants NSF ATM-0513116, ATM-0528634, and ATM-0449815, NASA NNG04GA67G and NNG06GB03G, UCAR/NSF S05-39607, and by EPA fellowship FP-91650801 (to PFD) and NASA fellowship NNG04GR06H (to ACA).

Edited by: S. Madronich

References

Aiken, A. C., Cubison, M. J., Huffman, J. A., DeCarlo, P. F., Ulbrich, I., Docherty, K., Sueper, D. T., and Jimenez, J. L.: Organic Aerosol Analysis with the Aerodyne High Resolution Time-of Flight Aerosol Mass Spectrometer (HR-ToF-AMS) at T0 in Mexico City during MILAGRO / MCMA-2006, American Association of Aerosol Research, Reno, NV, 2007a.

Aiken, A. C., DeCarlo, P. F., and Jimenez, J. L.: Elemental Analysis of Organic Species with Electron Ionization High-Resolution Mass Spectrometry, Anal. Chem., 79, 8350–8358, 2007b.

Aiken, A. C., DeCarlo, P. F., Kroll, J. H., Worsnop, D. R., Huffman, J. A., Docherty, K. S., Ulbrich, I. M., Mohr, C., Kimmel, J. R., Sueper, D., Sun, Y., Zhang, Q., Trimborn, A. M., Northway, M., Ziemann, P. J., Canagaratna, M. R., Onasch, T. B., Alfarra, M. R., Prevot, A. S. H., Dommen, J., Duplissy, J., Metzger, A., Baltensperger, U., and Jimenez, J. L.: O/C and OM/OC Ratios of Primary, Secondary, and Ambient Organic Aerosols with High-Resolution Time-of-Flight Aerosol Mass Spectrometry, Environ. Sci. Technol., 42, 4478–4485, 2008.

Alfarra, M. R., Coe, H., Allan, J. D., Bower, K. N., Boudries, H., Canagaratna, M. R., Jimenez, J. L., Jayne, J. T., Garforth, A. A., Li, S. M., and Worsnop, D. R.: Characterization of urban and rural organic particulate in the lower Fraser valley using two aerodyne aerosol mass spectrometers, Atmos. Environ., 38, 5745–5758, 2004.

Alfarra, M. R., Paulsen, D., Gysel, M., Garforth, A. A., Dommen, J., Prévôt, A. S. H., Worsnop, D. R., Baltensperger, U., and Coe, H.: A mass spectrometric study of secondary organic aerosols formed from the photooxidation of anthropogenic and biogenic precursors in a reaction chamber, Atmos. Chem. Phys. Discuss., 6, 7747–7789, 2006, http://www.atmos-chem-phys-discuss.net/6/7747/2006/.

Alfarra, M. R., Prevot, A. S. H., Szidat, S., Sandradewi, J., Weimer, S., Lanz, V. A., Schreiber, D., Mohr, M., and Baltensperger, U.: Identification of the Mass Spectral Signature of Organic Aerosols from Wood Burning Emissions, Environ. Sci. Technol., 41, 5770–5777, 2007.

Allan, J. D., Alfarra, M. R., Bower, K. N., Williams, P. I., Gallagher, M. W., Jimenez, J. L., McDonald, A. G., Nemitz, E., Canagaratna, M. R., Jayne, J. T., Coe, H., and Worsnop, D. R.: Quantitative Sampling Using an Aerodyne Aerosol Mass Spectrometer: 2. Measurements of Fine Particulate Chemical Composition in Two UK Cities, J. Geophys. Res.-Atmos., 108(D9), 4091, doi:10:1029/2002JD002359, 2003.

Allan, J. D., Delia, A. E., Coe, H., Bower, K. N., Alfarra, M. R., Jimenez, J. L., Middlebrook, A. M., Drewnick, F., Onasch, T. B., Canagaratna, M. R., Jayne, J. T., and Worsnopf, D. R.: A generalised method for the extraction of chemically resolved mass spectra from aerodyne aerosol mass spectrometer data, J. Aerosol Sci., 35, 909–922, 2004.

Anderson, T. L., Covert, D. S., Marshall, S. F., Laucks, M. L., Charlson, R. J., Waggoner, A. P., Ogren, J. A., Caldow, R., Holm, R. L., Quant, F. R., Sem, G. J., Wiedensohler, A., Ahlquist, N. A., and Bates, T. S.: Performance characteristics of a high-sensitivity, three-wavelength, total scatter/backscatter nephelometer, J. Atmos. Ocean. Tech., 13, 967–986, 1996.

Anderson, T. L. and Ogren, J. A.: Determining aerosol radiative properties using the TSI 3563 integrating nephelometer, Aerosol Sci. Tech., 29, 57–69, 1998.

Anderson, T. L., Masonis, S. J., Covert, D. S., Ahlquist, N. C., Howell, S. G., Clarke, A. D., and McNaughton, C. S.: Variability of aerosol optical properties derived from in situ aircraft measurements during ACE-Asia, J. Geophys. Res., 108(D23), 8647, doi:8610.1029/2002JD003247, 2003.

Bahreini, R., Dunlea, E. J., Matthew, B. M., Simons, C., Docherty, K. S., DeCarlo, P. F., Brock, C. A., Jimenez, J. L., and Middlebrook, A. M.: Design and Operation of a Pressure Controlled Inlet for Airborne Sampling with an Aerodyne Aerosol Mass Spectrometer, Aerosol Sci. Tech., 42, 6, 465–471, 2008.

Bohren, C. F. and Huffman, D. R.: Absorption and scattering of light by small particles, Wiley, New York, 530 pp., 1983.

Bravo, A. H., Sosa, E. R., Sanchez, A. P., Jaimes, P. M., and Saavedra, R. M. I.: Impact of wildfires on the air quality of Mexico City, 1992–1999, Environ. Pollut., 117, 243–253, 2002.

Bytnerowicz, A. and Fenn, M. E.: Nitrogen deposition in California forests: A review, Environ. Pollut., 92, 127–146, 1996.

Canagaratna, M. R., Jayne, J. T., Jimenez, J. L., Allan, J. D., Alfarra, M. R., Zhang, Q., Onasch, T. B., Drewnick, F., Coe, H., Middlebrook, A., Delia, A., Williams, L. R., Trimborn, A. M., Northway, M. J., DeCarlo, P. F., Kolb, C. E., Davidovits, P., and Worsnop, D. R.: Chemical and Microphysical Characterization of Ambient Aerosols with the Aerosol Mass Spectrometer, Mass Spectrom. Rev., 26, 185–222, 2007.

Crosier, J., Allan, J. D., Coe, H., Bower, K. N., Forment, P., and Williams, P. I.: Chemical composition of summertime aerosol in the Po Valley (Italy), northern Adriatic and Black Sea, Q. J. Roy. Meteor. Soc., 133, 61–75, 2007.

Cross, E. S., Slowik, J. G., Davidovits, P., Allan, J. D., Worsnop, D. R., Jayne, J. T., Lewis, D. K., Canagaratna, M., and Onasch, T. B.: Laboratory and ambient particle density determinations using light scattering in conjunction with aerosol mass spectrometry, Aerosol Sci. Tech., 41, 343–359, 2007.

Crounse, J. D., McKinney, K. A., Kwan, A. J., and Wennberg, P. O.: Measurement of gas-phase hydroperoxides by chemical ionization mass spectrometry, Anal. Chem., 78, 6726–6732, 2006.

de Foy, B., Varela, J. R., Molina, L. T., and Molina, M. J.: Rapid ventilation of the Mexico City basin and regional fate of the urban plume, Atmos. Chem. Phys., 6, 2321–2335, 2006, http://www.atmos-chem-phys.net/6/2321/2006/.

de Foy, B., Lei, W., Zavala, M., Volkamer, R., Samuelsson, J., Mellqvist, J., Galle, B., Martinez, A. P., Grutter, M., Retama, A., and Molina, L. T.: Modelling constraints on the emission inventory and on vertical dispersion for CO and SO2 in the Mexico City Metropolitan Area using Solar FTIR and zenith sky UV spectroscopy, Atmos. Chem. Phys., 7, 781–801, 2007, http://www.atmos-chem-phys.net/7/781/2007/.

de Foy, B., Fast, J. D., Paech, S. J., Phillips, D., Walters, J. T., Coulter, R. L., Martin, T. J., Pekour, M. S., Shaw, W. J., Kastendeuch, P. P., Marley, N. A., Retama, A., and Molina, L. T.: Basin-scale wind transport during the MILAGRO field campaign and comparison to climatology using cluster analysis, Atmos. Chem. Phys., 8, 1209–1224, 2008, http://www.atmos-chem-phys.net/8/1209/2008/.

de Gouw, J. A., Middlebrook, A. M., Warneke, C., Goldan, P. D., Kuster, W. C., Roberts, J. M., Fehsenfeld, F. C., Worsnop, D. R., Canagaratna, M. R., Pszenny, A. A. P., Keene, W. C., Marchewka, M., Bertman, S. B., and Bates, T. S.: Budget of organic carbon in a polluted atmosphere: Results from the New England Air Quality Study in 2002, J. Geophys. Res.-Atmos., 110, D16305, doi:10.1029/2004JD005623, 2005.

de Gouw, J. A., Brock, C. A., Atlas, E. L., Bates, T. S., Fehsenfeld, F. C., Goldan, P. D., Holloway, J. S., Kuster, W. C., Lerner, B. M., Matthew, B. M., Middlebrook, A. M., Onasch, T. B., Peltier, R. E., Quinn, P. K., Senff, C. J., Stohl, A., Sullivan, A. P., Trainer, M., Warneke, C., Weber, R. J., and Williams, E. J.: Sources of Particulate Matter in the Northeastern United States: 1. Direct Emissions and Secondary Formation of Organic Matter in Urban Plumes, J. Geophys. Res., 113, D08301, doi:08310.01029/02007JD009243, 2008.

DeCarlo, P., Slowik, J., Worsnop, D. R., Davidovits, P., and Jimenez, J.: Particle Morphology and Density Characterization by Combined Mobility and Aerodynamic Diameter Measurements. Part 1: Theory, Aerosol Sci. Tech., 38, 1185–1205, 2004.

DeCarlo, P. F., Kimmel, J. R., Trimborn, A., Northway, M. J., Jayne, J. T., Aiken, A. C., Gonin, M., Fuhrer, K., Horvath, T., Docherty, K. S., Worsnop, D. R., and Jimenez, J. L.: Field-deployable, high-resolution, time-of-flight aerosol mass spectrometer, Anal. Chem., 78, 8281–8289, 2006.

Docherty, K. S., Stone, E. A., Ulbrich, I. M., DeCarlo, P. F., Snyder, D. C., Schauer, J. J., Peltier, R. E., Weber, R. J., Murphy, S. M., Seinfeld, J. H., Eatough, D. J., and Jimenez, J. L.: Apportionment of Primary and Secondary Organic Aerosols in Southern California during the 2005 Study of Organic Aerosols in Riverside (SOAR), Environ. Sci. Technol., in press, 2008.

Drewnick, F., Hings, S. S., DeCarlo, P., Jayne, J. T., Gonin, M., Fuhrer, K., Weimer, S., Jimenez, J. L., Demerjian, K. L., Borrmann, S., and Worsnop, D. R.: A new time-of-flight aerosol mass spectrometer (TOF-AMS) – Instrument description and first field deployment, Aerosol Sci. Tech., 39(7), 637–658, 2005.

Dunlea, E. J., DeCarlo, P. F., Kimmel, J. R., Aiken, A. C., Peltier, R., Weber, R., Tomlinson, J., Collins, D., Shinozuka, Y., Howell, S., Clarke, A., Emmons, L., Apel, E., Pfister, G., van Donkelaar, A., Millet, D., Heald, C. L., and Jimenez, J. L.: Observations of Processed Asian Pollution with a High-Resolution Time-of-Flight Aerosol Mass Spectrometer (HR-ToF-AMS), Atmos. Chem. Phys. Discuss., in press, 2008.

Fast, J. D. and Zhong, S. Y.: Meteorological factors associated with inhomogeneous ozone concentrations within the Mexico City basin, J. Geophys. Res.-Atmos., 103, 18 927–18 946, 1998.

Fast, J. D., de Foy, B., Rosas, F. A., Caetano, E., Carmichael, G., Emmons, L., McKenna, D., Mena, M., Skamarock, W., Tie, X., Coulter, R. L., Barnard, J. C., Wiedinmyer, C., and Madronich, S.: A meteorological overview of the MILAGRO field campaigns, Atmos. Chem. Phys., 7, 2233–2257, 2007, http://www.atmos-chem-phys.net/7/2233/2007/.

Fountoukis, C., Nenes, A., Sullivan, A., Weber, R., VanReken, T., Fischer, M., Matv?as, E., Moya, M., Farmer, D., and Cohen, R. C.: Thermodynamic characterization of Mexico City aerosol during MILAGRO 2006, Atmos. Chem. Phys. Discuss., 7, 9203–9233, 2007, http://www.atmos-chem-phys-discuss.net/7/9203/2007/.

Gaffney, J. S., Marley, N. A., Sturchio, N. C., Heraty, L., Martinez, N., Hardy, K., and Guilderson, T.: Biogenic carbon dominance based on 13C/12C and 14C measurements of total carbon at T-0 and T-1 sites during MILAGRO, The 88th Annual Meeting of the American Meteorological Society New Orleans, LA, 20–24 January, abstract no. J1.1, 2008.

George, I. J., Slowik, J., and Abbatt, J. P. D.: Chemical aging of ambient organic aerosol from heterogeneous reaction with hydroxyl radicals, Geophys. Res. Lett., 35, L13811, doi:10.1029/2008GL033884, 2008.

Gerbig, C., Schmitgen, S., Kley, D., Volz-Thomas, A., Dewey, K., and Haaks, D.: An improved fast-response vacuum-UV resonance fluorescence CO instrument, J. Geophys. Res.-Atmos., 104, 1699–1704, 1999.

Grutter, M., Basaldud, R., Rivera, C., Harig, R., Junkerman, W., Caetano, E., and Delgado-Granados, H.: SO2 emissions from Popocatpetl volcano: emission rates and plume imaging using optical remote sensing techniques, Atmos. Chem. Phys. Discuss., 8, 8119–8141, 2008, http://www.atmos-chem-phys-discuss.net/8/8119/2008/.

Gysel, M., Crosier, J., Topping, D. O., Whitehead, J. D., Bower, K. N., Cubison, M. J., Williams, P. I., Flynn, M. J., McFiggans, G. B., and Coe, H.: Closure study between chemical composition and hygroscopic growth of aerosol particles during TORCH2, Atmos. Chem. Phys., 7, 6131–6144, 2007, http://www.atmos-chem-phys.net/7/6131/2007/.

Hand, J. L., Kreidenweis, S. M., Kreisberg, N., Hering, S., Stolzenburg, M., Dick, W., and McMurry, P. H.: Comparisons of Aerosol Properties Measured by Impactors and Light Scattering from Individual Particles: Refractive Index, Number and Volume Concentrations, and Size Distributions, Atmos. Environ., 36, 1853–1861, 2002.

Heald, C. L., Jacob, D. J., Park, R. J., Russell, L. M., Huebert, B. J., Seinfeld, J. H., Liao, H., and Weber, R. J.: A large organic aerosol source in the free troposphere missing from current models, Geophys. Res. Lett., 32, L18809, doi:10.1029/2005GL023831, 2005.

Heintzenberg, J., and Charlson, R. J.: Design and Applications of the Integrating Nephelometer: A Review, J. Atmos. Ocean. Tech., 13, 987–1000, 1996.

Huffman, J. A., Ziemann, P. J., Jayne, J. T., Worsnop, D. R., and Jimenez, J. L.: Development and Characterization of a Fast-Stepping/Scanning Thermodenuder for Chemically-Resolved Aerosol Volatility Measurements, Aerosol Sci. Tech., 42, 395–407, 2008b.

IPCC: Climate Change 2007: The Scientific Basis. Contribution of Working Group I to the Fourth Assessment Report of the Intergovernmental Panel on Climate Change, edited by: Solomon, S., Qin, D., Manning, M., Marquis, M., Averyt, K., Tignor, M. M. B., Miller, H. L., and Chen, Z., Cambridge University Press, Cambridge, England, 2007.

Jayne, J. T., Leard, D. C., Zhang, X. F., Davidovits, P., Smith, K. A., Kolb, C. E., and Worsnop, D. R.: Development of an Aerosol Mass Spectrometer for Size and Composition Analysis of Submicron Particles, Aerosol Sci. Tech., 33, 49–70, 2000.

Jimenez, J. L., Jayne, J. T., Shi, Q., Kolb, C. E., Worsnop, D. R., Yourshaw, I., Seinfeld, J. H., Flagan, R. C., Zhang, X. F., Smith, K. A., Morris, J. W., and Davidovits, P.: Ambient Aerosol Sampling using the Aerodyne Aerosol Mass Spectrometer, J. Geophys. Res.-Atmos., 108(D7), 8425, doi:8410.1029/2001JD001213, 2003.

Johnson, D., Utembe, S. R., Jenkin, M. E., Derwent, R. G., Hayman, G. D., Alfarra, M. R., Coe, H., and McFiggans, G.: Simulating regional scale secondary organic aerosol formation during the TORCH 2003 campaign in the southern UK, Atmos. Chem. Phys., 6, 403–418, 2006a, http://www.atmos-chem-phys.net/6/403/2006/.

Johnson, K. S., de Foy, B., Zuberi, B., Molina, L. T., Molina, M. J., Xie, Y., Laskin, A., and Shutthanandan, V.: Aerosol composition and source apportionment in the Mexico City Metropolitan Area with PIXE/PESA/STIM and multivariate analysis, Atmos. Chem. Phys., 6, 4591–4600, 2006b, http://www.atmos-chem-phys.net/6/4591/2006/.

Kimmel, J., DeCarlo, P. F., Trimborn, A. M., Northway, M. J., Worsnop, D. R., and Jimenez, J. L.: Quantitative Time-of-flight Mass Spectrometry of Aerosols Using a Digitally Thresholded Analog-to-Digital Converter, American Society for Mass Spectrometry, Seattle, Washington, http://cires.colorado.edu/jimenez-group/ToFAMSResources/ToFManual/Docs/Kimmel_ASMS_2006.pdf, 2006.

Kleinman, L. I., Daum, P. H., Lee, Y. N., Senum, G. I., Springston, S. R., Wang, J., Berkowitz, C., Hubbe, J., Zaveri, R. A., Brechtel, F. J., Jayne, J., Onasch, T. B., and Worsnop, D.: Aircraft observations of aerosol composition and ageing in New England and Mid-Atlantic States during the summer 2002 New England Air Quality Study field campaign, J. Geophys. Res.-Atmos., 112, D09310, doi:10.1029/2006JD007786, 2007.

Kleinman, L. I., Springston, S. R., Daum, P. H., Lee, Y. N., Nunnermacker, L. J., Senum, G. I., Wang, J., Weinstein-Lloyd, J., Alexander, M. L., Hubbe, J., Ortega, J., Canagaratna, M. R., and Jayne, J.: The time evolution of aerosol composition over the

Mexico City plateau, Atmos. Chem. Phys., 8, 1559–1575, 2008, http://www.atmos-chem-phys.net/8/1559/2008/.

Lawrence, M. G., Butler, T. M., Steinkamp, J., Gurjar, B. R., and Lelieveld, J.: Regional pollution potentials of megacities and other major population centers, Atmos. Chem. Phys., 7, 3969–3987, 2007, http://www.atmos-chem-phys.net/7/3969/2007/.

Lee, T., Sullivan, A. P., Collett, J. L., Kreidenweis, S. M., Jimenez, J. L., Onasch, T. B., Trimborn, A. M., Malm, W. C., Hao, W. M., and Wold, C.: Characterizing of the chemical properties of biomass combustion smoke using an aerosol mass spectrometer, Annual Conference of the Air and Waste Management Association, Portland, OR, 2008.

Madronich, S.: Chemical evolution of gaseous air pollutants downwind of tropical megacities: Mexico City case study, Atmos. Environ., 40, 6012–6018, 2006.

Maring, H., Savoie, D. L., Izaguirre, M. A., Custals, L., and Reid, J. S.: Mineral dust aerosol size distribution change during atmospheric transport, J. Geophys. Res., 108, 8592, doi:8510.1029/2002JD002536, 2003.

McNaughton, C. S., Clarke, A. D., Howell, S. G., Pinkerton, M., Anderson, B., Thornhill, L., Hudgins, C., Winstead, E., Dibb, J. E., Scheuer, E., and Maring, H.: Results from the DC-8 Inlet Characterization Experiment (DICE): Airborne versus surface sampling of mineral dust and sea salt aerosols, Aerosol Sci. Tech., 41, 136–159, 2007.

Moffet, R. C., de Foy, B., Molina, L. T., Molina, M. J., and Prather, K. A.: Measurement of ambient aerosols in northern Mexico City by single particle mass spectrometry, Atmos. Chem. Phys. Discuss., 7, 6413–6457, 2007, http://www.atmos-chem-phys-discuss.net/7/6413/2007/.

Molina, L. T., Kolb, C. E., de Foy, B., Lamb, B. K., Brune, W. H., Jimenez, J. L., Ramos-Villegas, R., Sarmiento, J., Paramo-Figueroa, V. H., Cardenas, B., Gutierrez-Avedoy, V., and Molina, M. J.: Air quality in North America's most populous city – overview of the MCMA-2003 campaign, Atmos. Chem. Phys., 7, 2447–2473, 2007, http://www.atmos-chem-phys.net/7/2447/2007/.

Molina, M. J., Ivanov, A. V., Trakhtenberg, S., and Molina, L. T.: Atmospheric evolution of organic aerosol, Geophys. Res. Lett., 31, L22104, doi:10.1029/2004GL020910, 2004.

Morino, Y., Kondo, Y., Takegawa, N., Miyazaki, Y., Kita, K., Komazaki, Y., Fukuda, M., Miyakawa, T., Moteki, N., and Worsnop, D. R.: Partitioning of HNO3 and particulate nitrate over Tokyo: Effect of vertical mixing, J. Geophys. Res.-Atmos., 111, D15215, doi:10.1029/2005JD006887, 2006.

Murphy, D. M., Cziczo, D. J., Hudson, P. K., and Thomson, D. S.: Carbonaceous material in aerosol particles in the lower stratosphere and tropopause region, J. Geophys. Res.-Atmos., 112, D04203, doi:10.1029/2006JD007297, 2007.

Neuman, J. A., Nowak, J. B., Brock, C. A., Trainer, M., Fehsenfeld, F. C., Holloway, J. S., Hubler, G., Hudson, P. K., Murphy, D. M., Nicks, D. K., Orsini, D., Parrish, D. D., Ryerson, T. B., Sueper, D. T., Sullivan, A., and Weber, R.: Variability in ammonium nitrate formation and nitric acid depletion with altitude and location over California, J. Geophys. Res.-Atmos., 108, 4557, doi:10.1029/2003JD003616, 2003.

Park, K., Kittelson, D. B., Zachariah, M. R., and McMurry, P. H.: Measurement of Inherent Material Density of Nanoparticle Agglomerates, J. Nanopart. Res., 6, 267–272, 2004.

Peltier, R. E., Sullivan, A. P., Weber, R. J., Brock, C. A., Wollny, A. G., Holloway, J. S., Gouw, J. A. d., and Warneke, C.: Fine aerosol bulk composition measured on WP-3D research aircraft in vicinity of the Northeastern United States – results from NEAQS, Atmos. Chem. Phys., 7, 3231–3247, 2007a, http://www.atmos-chem-phys.net/7/3231/2007/.

Peltier, R. E., Sullivan, A. P., Weber, R. J., Wollny, A. G., Holloway, J. S., Brock, C. A., de Gouw, J. A., and Atlas, E. L.: No evidence for acid-catalyzed secondary organic aerosol formation in power plant plumes over metropolitan Atlanta, Georgia, Geophys. Res. Lett., 34, L06801, doi:10.1029/2006GL028780, 2007b.

Pope, C. A., and Dockery, D. W.: Health effects of fine particulate air pollution: lines that connect, J. Air Waste Manage., 56, 709–742, 2006.

Querol, X., Pey, J., Minguillón, M. C., Pérez, N., Alastuey, A., Viana1, M., Moreno, T., Bernabé, R. M., Blanco, S., Cárdenas, B., Vega, E., Sosa, G., Escalona, S., Ruiz, H., and Artíñano, B.: PM speciation and sources in Mexico during the MILAGRO-2006 Campaign, Atmos. Chem. Phys., 8, 111–128, 2008, http://www.atmos-chem-phys.net/8/111/2008/.

Quinn, P. K., Bates, T. S., Coffman, D., Onasch, T. B., Worsnop, D., Baynard, T., de Gouw, J. A., Goldan, P. D., Kuester, W. C., Williams, E., Roberts, J. M., Lerner, B., Stohl, A., Pettersson, A., and Lovejoy, E. R.: Impacts of Sources and Aging on Submicrometer Aerosol Properties in the Marine Boundary Layer Across the Gulf of Maine, J. Geophys. Res., 111, D23S36, doi:10.1029/2006JD007582, 2006.

Raga, G. B., Kok, G. L., Baumgardner, D., Baez, A., and Rosas, I.: Evidence for volcanic influence on Mexico City aerosols, Geophys. Res. Lett., 26, 1149–1152, 1999.

Raga, G. B., Baumgardner, D., Castro, T., Martinez-Arroyo, A., and Navarro-Gonzalez, R.: Mexico City air quality: a qualitative review of gas and aerosol measurements (1960–2000), Atmos. Environ., 35, 4041–4058, 2001.

Ridley, B., Ott, L., Pickering, K., Emmons, L., Montzka, D., Weinheimer, A., Knapp, D., Grahek, F., Li, L., Heymsfield, G., McGill, M., Kucera, P., Mahoney, M. J., Baumgardner, D., Schultz, M., and Brasseur, G.: Florida thunderstorms: A faucet of reactive nitrogen to the upper troposphere, J. Geophys. Res.-Atmos., 109, D17305, doi:10.1029/2004JD004769, 2004.

Salcedo, D., Onasch, T. B., Dzepina, K., Canagaratna, M. R., Zhang, Q., Huffman, J. A., DeCarlo, P. F., Jayne, J. T., Mortimer, P., Worsnop, D. R., Kolb, C. E., Johnson, K. S., Zuberi, B., Marr, L. C., Volkamer, R., Molina, L. T., Molina, M. J., Cardenas, B., Bernabe, R. M., Marquez, C., Gaffney, J. S., Marley, N. A., Laskin, A., Shutthanandan, V., Xie, Y., Brune, W., Lesher, R., Shirley, T., and Jimenez, J. L.: Characterization of ambient aerosols in Mexico City during the MCMA-2003 campaign with Aerosol Mass Spectrometry: results from the CENICA Supersite, Atmos. Chem. Phys., 6, 925–946, 2006, http://www.atmos-chem-phys.net/6/925/2006/.

San Martini, F. M., Dunlea, E. J., Volkamer, R., Onasch, T. B., Jayne, J. T., Canagaratna, M. R., Worsnop, D. R., Kolb, C. E., Shorter, J. H., Herndon, S. C., Zahniser, M. S., Salcedo, D., Dzepina, K., Jimenez, J. L., Ortega, J. M., Johnson, K. S., McRae, G. J., Molina, L. T., and Molina, M. J.: Implementation

of a Markov Chain Monte Carlo method to inorganic aerosol modeling of observations from the MCMA-2003 campaign – Part II: Model application to the CENICA, Pedregal and Santa Ana sites, Atmos. Chem. Phys., 6, 4889–4904, 2006, http://www.atmos-chem-phys.net/6/4889/2006/.

Schauer, J. J., Rogge, W. F., Hildemann, L. M., Mazurek, M. A., and Cass, G. R.: Source apportionment of airborne particulate matter using organic compounds as tracers, Atmos. Environ., 30, 3837–3855, 1996.

Schneider, J., Weimer, S., Drewnick, F., Borrmann, S., Helas, G., Gwaze, P., Schmid, O., Andreae, M. O., and Kirchner, U.: Mass spectrometric analysis and aerodynamic properties of various types of combustion-related aerosol particles, Int. J. Mass Spectrom., 258, 37–49, 2006.

Seinfeld, J. H., and Pandis, S. N.: Atmospheric chemistry and physics : from air pollution to climate change, Wiley, New York, xxvii, 1326 pp., 1998.

Shinozuka, Y., Clarke, A. D., Howell, S. G., Kapustin, V. N., McNaughton, C. S., Zhou, J. C., and Anderson, B. E.: Aircraft profiles of aerosol microphysics and optical properties over North America: Aerosol optical depth and its association with PM2.5 and water uptake, J. Geophys. Res.-Atmos., 112, D12S20, doi:10.1029/2006JD007918, 2007.

Smithsonian Global Volcanism Program: Volcanoes of Mexico and Central America, http://www.volcano.si.edu/world/region.cfm?rnum=1401, 2007.

Stolzenburg, M., Kreisberg, N., and Hering, S.: Atmospheric size distributions measured by differential mobility optical particle size spectrometry, Aerosol Sci. Tech., 29, 402–418, 1998.

Stone, E. A., Snyder, D. C., Sheesley, R. J., Sullivan, A. P., Weber, R. J., and Schauer, J. J.: Source apportionment of fine organic aerosol in Mexico City during the MILAGRO Experiment 2006, Atmos. Chem. Phys., 8, 1249–1259, 2008, http://www.atmos-chem-phys.net/8/1249/2008/.

Takegawa, N., Miyazaki, Y., Kondo, Y., Komazaki, Y., Miyakawa, T., Jimenez, J. L., Jayne, J. T., Worsnop, D. R., Allan, J. D., and Weber, R. J.: Characterization of an Aerodyne Aerosol Mass Spectrometer (AMS): Intercomparison with other aerosol instruments, Aerosol Sci. Tech., 39, 760–770, 2005.

Tanaka, P. L., Riemer, D. D., Chang, S. H., Yarwood, G., McDonald-Buller, E. C., Apel, E. C., Orlando, J. J., Silva, P. J., Jimenez, J. L., Canagaratna, M. R., Neece, J. D., Mullins, C. B., and Allen, D. T.: Direct evidence for chlorine-enhanced urban ozone formation in Houston, Texas, Atmos. Environ., 37, 1393–1400, 2003.

Ulbrich, I. M., Canagaratna, M. R., Zhang, Q., Worsnop, D. R., and Jimenez, J. L.: Interpretation of Organic Components from Positive Matrix Factorization of Aerosol Mass Spectrometric Data. , Atmos. Chem. Phys. Discuss., 8, 6729–6791, 2008, http://www.atmos-chem-phys-discuss.net/8/6729/2008/.

Volkamer, R., Jimenez, J. L., San Martini, F., Dzepina, K., Zhang, Q., Salcedo, D., Molina, L. T., Worsnop, D. R., and Molina, M. J.: Secondary organic aerosol formation from anthropogenic air pollution: Rapid and higher than expected, Geophys. Res. Lett., 33, L17811, doi:10.1029/2006GL026899., 2006.

Volkamer, R., San Martini, F., Molina, L. T., Salcedo, D., Jimenez, J. L., and Molina, M. J.: A Missing Sink for Gas-Phase Glyoxal in Mexico City: Formation of Secondary Organic Aerosol, Geophys. Res. Lett., 34, L19807, doi:19810.11029/12007GL030752, 2007.

Wang, S. C. and Flagan, R. C.: Scanning Electrical Mobility Spectrometer, Aerosol Sci. Tech., 13, 230–240, 1990.

Watson, J. G.: Visibility: Science and regulation, J. Air Waste Manage., 52, 628–713, 2002.

Yokelson, R., Urbanski, S., Atlas, E., Toohey, D., Alvarado, E., Crounse, J., Wennberg, P., Fisher, M., Wold, C., Campos, T., Adachi, K., Buseck, P. R., and Hao, W. M.: Emissions from forest fires near Mexico City, Atmos. Chem. Phys., 7, 5569–5584, 2007, http://www.atmos-chem-phys.net/7/5569/2007/.

Zhang, Q., Stanier, C. O., Canagaratna, M. R., Jayne, J. T., Worsnop, D. R., Pandis, S. N., and Jimenez, J. L.: Insights into the chemistry of new particle formation and growth events in Pittsburgh based on aerosol mass spectrometry, Environ. Sci. Technol., 38, 4797–4809, 2004.

Zhang, Q., Alfarra, M. R., Worsnop, D. R., Allan, J. D., Coe, H., Canagaratna, M. R., and Jimenez, J. L.: Deconvolution and Quantification of Primary and Oxygenated Organic Aerosols Based on Aerosol Mass Spectrometry. Part 1: Development and Validation of the Method, Environ. Sci. Technol., 39, 4938–4952, 2005a.

Zhang, Q., Canagaratna, M. R., Jayne, J. T., Worsnop, D. R., and Jimenez, J. L.: Time and Size-Resolved Chemical Composition of Submicron Particles in Pittsburgh – Implications for Aerosol Sources and Processes, J. Geophys. Res.-Atmos., 110, D07S09, doi:10.1029/2004JD004649, 2005b.

Zhang, Q., Worsnop, D. R., Canagaratna, M. R., and Jimenez, J. L.: Hydrocarbon-like and oxygenated organic aerosols in Pittsburgh: insights into sources and processes of organic aerosols, Atmos. Chem. Phys., 5, 3289–3311, 2005c, http://www.atmos-chem-phys.net/5/3289/2005/.

Zhang, Q., Jimenez, J. L., Canagaratna, M. R., Allan, J. D., Coe, H., Ulbrich, I., Alfarra, M. R., Takami, A., Middlebrook, A. M., Sun, Y. L., Dzepina, K., Dunlea, E., Docherty, K., DeCarlo, P. F., Salcedo, D., Onasch, T., Jayne, J. T., Miyoshi, T., Shimono, A., Hatakeyama, S., Takegawa, N., Kondo, Y., Schneider, J., Drewnick, F., Borrmann, S., Weimer, S., Demerjian, K., Williams, P., Bower, K., Bahreini, R., Cottrell, L., Griffin, R. J., Rautiainen, J., Sun, J. Y., Zhang, Y. M., and Worsnop, D. R.: Ubiquity and dominance of oxygenated species in organic aerosols in anthropogenically-influenced Northern Hemisphere midlatitudes, Geophys. Res. Lett., 34, L13801, doi:13810.11029/12007GL029979, 2007a.

Zhang, Q., Jimenez, J. L., Worsnop, D. R., and Canagaratna, M.: A Case Study of Urban Particle Acidity and Its Influence on Secondary Organic Aerosol, Environ. Sci. Technol., 41, 3213–3219, 2007b.